Differentiation of Benign and Malignant Vertebral Compression Fractures

Andrea Baur-Melnyk and Tobias Geith

Contents

Abstract

The differentiation between acute benign osteoporotic and malignant vertebral fractures is sometimes challenging, since they both occur without adequate trauma and are common in the elderly population. Conventional X-ray is the first imaging method to depict vertebral fractures, however it lacks specificity. CT allows better delineation of osseous destruction in neoplastic fractures, however it is not always possible to define the exact cause of the fracture. MRI is more specific as well as more sensitive in detecting especially discrete osteoporotic fractures. In most cases the combination of morphological signs in CT and MRI allows the determination of a benign or malignant cause of the vertebral fracture. However, there remain uncertain cases with contradictory imaging features. In the following chapter, we discuss the morphological signs which help in the differentiation between acute benign and neoplastic vertebral fractures. We describe the latest techniques such as diffusion-weighted, chemical-shift, and perfusion MRI as well as nuclear-medical techniques.

1   Epidemiology and Clinical Background

Vertebral compression fractures occurring without adequate trauma are a common clinical problem. The most common cause of benign vertebral compression fractures is osteoporosis. The European Vertebral Osteoporosis Study (EVOS) examined radiographs of 15,570 males and females aged 50–79 years in 19

A. Baur-Melnyk (✉) · T. Geith
Institut für Klinische Radiologie,
Klinikum der Universität Munchen-Großhadern,
Marchioninistraße 15, 81377 Munich, Germany
e-mail: Andrea.Baur@med.uni-muenchen.de

European countries and showed a prevalence of osteoporotic vertebral fractures ranging from 6 to 21%, with a prevalence of 15.1% in men (mean age 64.0 years) and 17.2% in women (mean age 65.5 years) (O'Neill et al. 1996). Since many vertebral fractures escape clinical diagnosis, and because back pain is a common complaint in the elderly, it is difficult to establish a reliable epidemiology. Menopause, advanced age, and a maternal history of fractures are associated with lower bone density, which leads to an increased risk of osteoporotic fractures (Melton 1997). The yearly incidence of vertebral fracture in women rises from 0.6% at an age between 55 and 57 years to 2.3% at an age between 75 and 79 years (van der Klift et al. 2004). Estrogen deficiency is the most important factor in the pathogenesis of vertebral osteoporosis, with environmental or genetic factors also appearing to be contributory factors (O'Neill et al. 1996).

Metastatic lesions are the most common tumors of the spine (95–98%). The spine is the third most frequent place of metastatic deposits, following the lung and the liver. Forty percent of cancer patients have spinal metastases, 10–20% of them are symptomatic (Harrington 1986; White et al. 2006). The metastatic seeding occurs mainly through the arterial blood supply, a retrograde spread through the Batson plexus is also possible (Batson 1940).

In a study on 600 cases of spinal metastases, the most frequent primary cancers were cancers of the prostate and the reproductive system (21%), the lung (19%), and sarcoma (9%) in men, and breast cancer (53%), uterus cancer (9%) and hematological malignancies (5%) in women (Constans et al. 1983). Multiple myeloma or solitary plasmocytoma and lymphoma are also common (Cuenod et al. 1996).

About 70% of symptomatic lesions are found in the thoracic region of the spine, particularly at the level of T4–T7. Twenty percent are found in the lumbar region and 10% are found in the cervical spine. More than 50% of patients with spinal metastasis have several levels of involvement. About 10–38% of patients have involvement of several noncontiguous segments.

One-third of cancer patients also have osteoporotic fractures without malignant infiltration (Fornasier and Czitrom 1978). A correct diagnosis is crucial for appropriate clinical staging, treatment, and prognostic determination, if a new vertebral fracture appears in these patients (Jung et al. 2003).

2 Conventional Imaging Techniques in the Differentiation of Benign Versus Malignant Vertebral Fractures

2.1 Plain Film Radiographs

Conventional radiographs of the spine are the standard technique in assessing vertebral fractures. The age of a fracture is difficult to be determined on plain film radiographs. An increased density due to impaction of trabeculae adjacent to the endplate and cortical disruption are signs of more recent, acute fractures. Subacute fractures show callus formation along the endplate. Osteoporotic fractures may only show minimal increase in density, because the overall bone density is already low. MRI is more sensitive, showing bone marrow edema in acute and subacute fractures (Link et al. 2005).

Vertebral compression fractures are classified as crush, wedge (loss of anterior vertebral body height with relative preservation of posterior body height), and end-plate fractures. Wedge-type fractures may lead to increased segmental kyphosis (Wasnich 1996).

Genant et al. (1993) evaluated vertebral fractures in plain film radiographs and semi-quantitatively characterized vertebral bodies as follows (Fig. 1):

- Grade 0 shows no fracture without reduction in vertebral height.
- Grade 1 describes a mild fracture with a reduction in vertebral height of 20–25%, compared with adjacent normal vertebrae.
- Grade 2 shows a moderate fracture with a reduction in height of 25–40%.
- Grade 3 represents a severe fracture with a reduction in height of more than 40%.

The discrimination of an osteoporotic from a malignant vertebral body fracture is limited in plain film radiographs.

Signs of osteoporotic vertebral fractures are the typical localization in the middle thoracic and the upper lumbar spine, a typical "fish-mouth" or "wedge-shaped" vertebra, further vertebral compression fractures, an intravertebral vacuum phenomenon and band-like sclerosis adjacent to the vertebral endplates. A concave posterior border is more likely a sign of an osteoporotic fracture, especially if there is some retropulsion of osseous

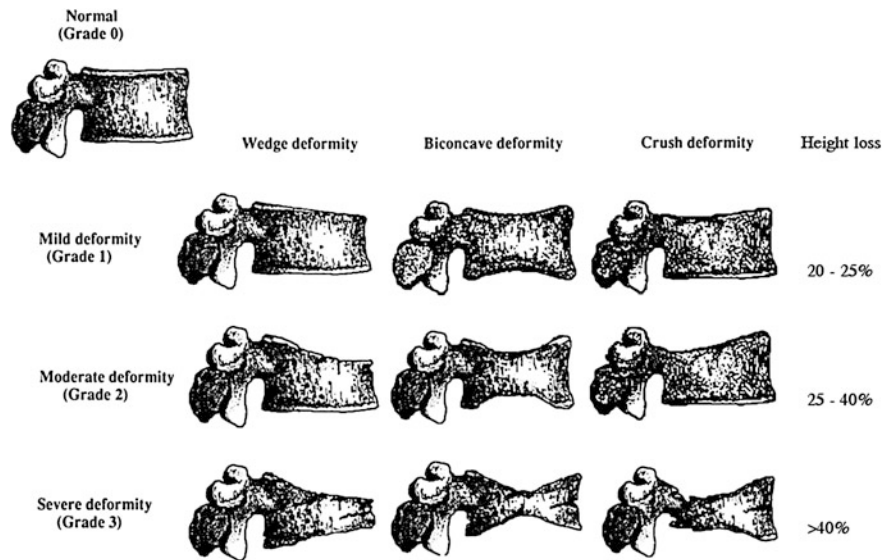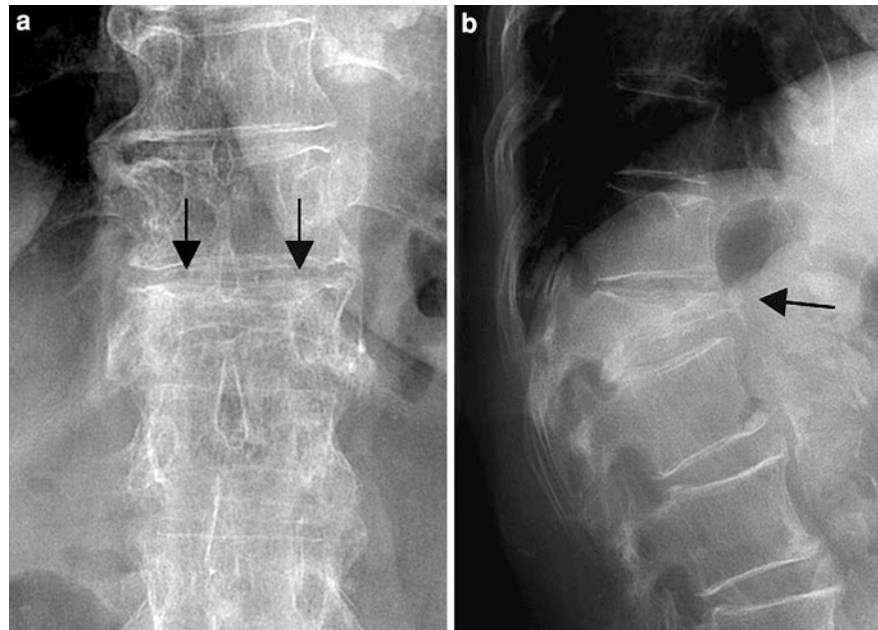Fig. 1 Spinal fracture index according to Genant et al. (1993)

Fig. 2 65-year-old patient with a typical osteoporotic fracture of Th 12. **a** A.p. radiograph showing a symmetric infraction, since the whole vertebral body is weakened; **b** lateral radiograph showing a severe wedge deformity (Genant Grade 3)

fragments into the spinal canal. Osteoporotic fractures usually show a more symmetric infraction of the endplates without osteolyses, since the whole vertebral body is weakened (Laredo et al. 1995; Link et al. 2005). Figure 2 shows the a.p. and lateral radiographs of a typical osteoporotic vertebral fracture.

Signs of malignancy are an inhomogeneous osseous structure with osteolyses and sclerotic areas as a sign of metastatic affection, a convex posterior border, involvement of the pedicles (vanished "eyes of the

vertebra"; Fig. 3a), fractures of the posterior part of the vertebral body, a paraspinal soft tissue mass, and localization above Th 7. An asymmetric height loss in antero-posterior (a.-p.)-projection is also a sign of malignancy, since an osteolysis is often asymmetrically located at one side of the vertebra (Sartoris et al. 1986; Link et al. 2005). Figure 3 shows the a.p. and lateral radiographs of a typical malignant vertebral fracture.

Table 1 gives an overview of the X-ray and CT features of benign and malignant vertebral fractures.

Fig. 3 55-year-old patient with a typical malignant fracture of L2. **a** A.p. radiograph showing an asymmetric infraction (*arrow*) and involvement of the left pedicle (vanished "eye of the vertebra") (*arrowheads*); **b** lateral radiograph showing an angling of the end-plate (arrow)
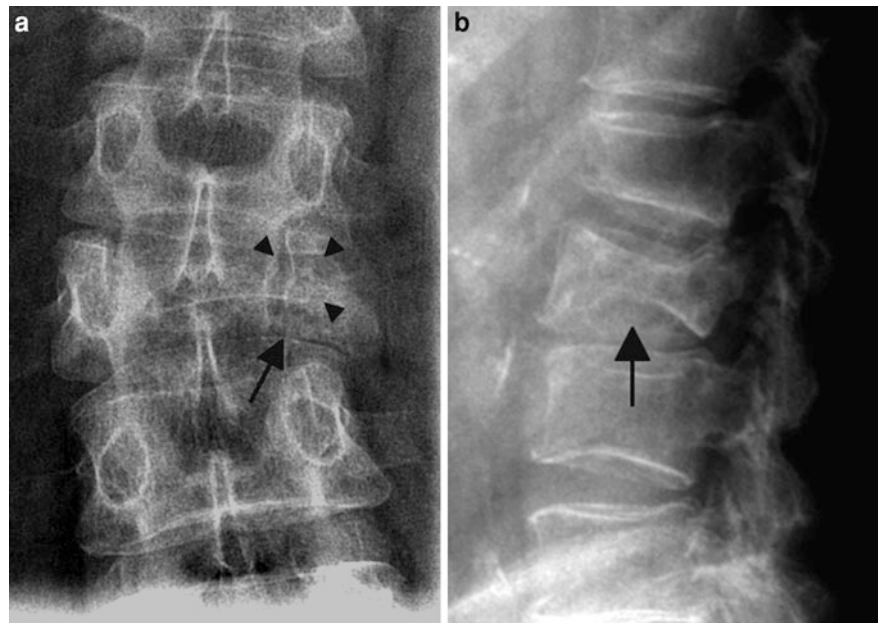
Sartoris et al. (1986) examined the radiographic patterns of 99 autopsy specimens with vertebral body collapse and endplate deformity of the thoracolumbar spine and found that angling of endplates was highly predictive of a malignant cause, whereas concavity was more suggestive of a benign disease. Focal versus diffuse involvement, the position of the apex of collapse, the condition of adjacent disks, and level of involvement within the spine appeared to be less important differentiation features.

However it must be stated, that in most cases a reliable distinction between acute benign and malignant vertebral compression fractures is not possible with plain film radiographs only.

2.2 Computed Tomography

In comparison with plain film radiographs, CT as a cross sectional method has a higher sensitivity and specificity. It is well-suited to assess the stability of an osteolytic lesion or fracture since it directly visualizes the osseous structures and demonstrates fracture lines in detail, but is less sensitive than MRI in depicting bone marrow and soft tissue pathology.

Sagittal and coronal reformations are fundamental for the differentiation between benign and malignant vertebral compression fractures. Early studies showed a weaker diagnostic accuracy of some morphologic CT signs (Laredo et al. 1995), presumably because they used only axial CT images with relatively thick slices (5 mm), whereas newer studies (Kubota et al. 2005) used axial images as well as sagittal and coronal multiplanar reconstructions with a thinner slice thickness of 0.7–1 mm, and therefore had a more detailed view of the fractures.
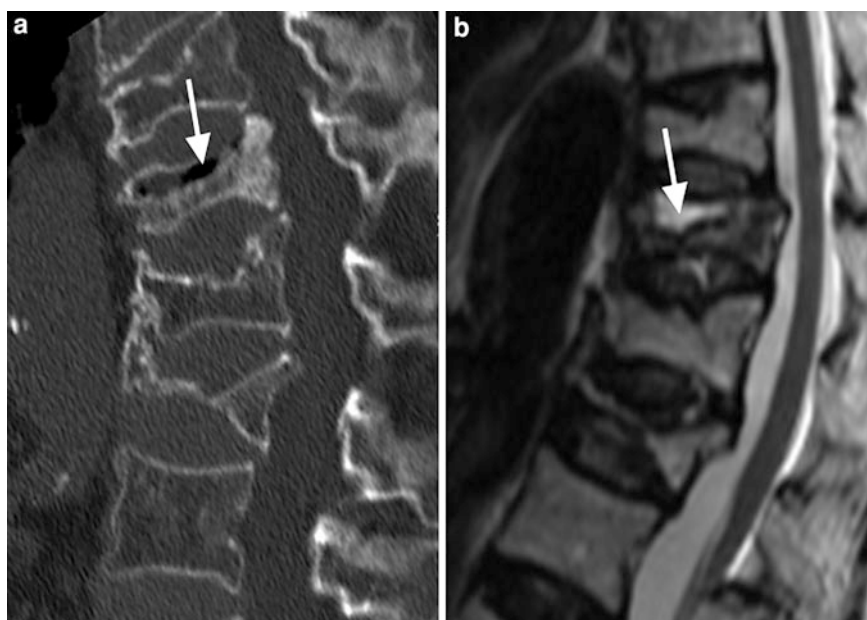
Osteoporotic fractures

Laredo et al. (1995) evaluated the CT findings in 34 benign and 32 malignant cases of nontraumatic acute vertebral collapse. *Cortical fractures without associated cortical destruction* (called "*puzzle sign*") were an almost constant finding in osteoporotic fractures and rather specific, since they were only seen in 9% of the malignant fractures. Another study by Kubota et al. (2005) revealed an accuracy up to 98.7% (sensitivity 97.8%, specificity 100%) for fractures of the anterolateral and/or posterior cortex without any cortical destruction of the vertebral body as a very reliable sign of a benign fracture.

Retropulsed bone fragments (Fig. 8a) of the superior or posterior corner of the vertebral body are very specific for an osteoporotic fracture (specificity up to 97%), and must be distinguished from a diffuse bulging of the posterior cortex, which is a rather common finding in malignant vertebral collapse (Laredo et al. 1995).

Table 1 *X-ray* and *CT features* of benign and malignant vertebral fractures

Benign osteoporotic fracture	Malignant fracture
Localization in middle thoracic and upper lumbar spine below Th 7	Localization above Th 7
Concave posterior border—retropulsion of bony fragments	Convex posterior border (bulging)
Intravertebral vacuum	No intravertebral vacuum—soft tissue density
Symmetric infraction (in a.p. view), wedge-shaped or fish-like vertebra	Asymmetric infraction (in a.p. view), Involvement of the pedicles (vanished "eyes of the vertebra")
Homogeneous osseous structure	Inhomogeneous osseous structure with osteolyses and sclerotic areas
Band-like sclerosis adjacent to vertebral cover plate	Fractures of the posterior part of the vertebra

Fig. 4 72-year-old patient with an osteoporotic fracture. **a** Sagittal CT in bone window showing the intravertebral vacuum (*arrow*); **b** corresponding T2-w MRI showing the "fluid sign" with a fluid-like hyperintense signal intensity (*arrow*) in the fractured vertebral body. The intravertebral vacuum and the intravertebral fluid are typical signs for the benign cause of the fracture

Fracture lines within the vertebral body are, although non-specific, a suggestive finding of an osteoporotic fracture, as well as defined margins of the fracture lines which are suggestive of a benign origin (Laredo et al. 1995).

Noninfectious gas collections in preformed or artificial areas of the vertebral body, where normally no gas accumulations are found, are called *vacuum phenomena*. They can be observed in various joints without having pathological relevance and are often seen in degenerative intervertebral discs. Patients with osteoporosis have a low vascularization and a high fat content of the vertebral bone marrow. The exact mechanism of the intravertebral vacuum cleft (Fig. 4) is still controversial. It is assumed that the formation of gas in the vertebral body is a reaction to the negative pressure, which arises when the initially compressed trabecular bone is partially distracted due to movement forces (Stäbler et al. 1999). There is possibly some form of pseudarthrosis following osteonecrosis (Hasegawa et al. 1998). The intravertebral vacuum cleft may be a stable phenomenon (Lafforgue et al. 1997) or can be replaced by fluid on MRI after supine positioning of the patient (Fig. 4) (Malghem et al. 1993; Linn et al. 2009).

Several studies on osteoporotic and malignant vertebral fractures found the intravertebral vacuum phenomenon only in cases of osteoporotic fractures (Golimbu et al. 1986; Laredo et al. 1995; Kubota et al. 2005). Exceptions are fractures in patients with plasmacytoma, where intravertebral vacuum has also been detected (Resnick et al. 1981; Kumpan et al. 1986;

Fig. 5 67-year-old patient with breast cancer and typical metastatic fractures of Th 9–11 and metastasis in L1. **a** STIR image showing the posterior cortical bulging with narrowing of the spinal canal (*arrows*). Further metastasis in the non-fractured L1 (*asterisk*); **b** corresponding T2-w image; **c** sagittal CT in bone window showing cortical destruction and destruction of the cancellous bone; **d** corresponding CT in soft-tissue window showing the cortical destruction and a soft-tissue mass (*arrows*). Intradiscal (not intravertebral!) vacuum (*arrowheads*) due to osteochondrosis; **e** axial CT of Th 10 in bone window showing a cortical destruction (*arrow*); **f** corresponding axial CT in soft-tissue window showing the soft-tissue mass that causes cortical destruction (*asterisk*)

Gagnerie et al. 1987). Other extremely rare cases of intravertebral gas are infections with gas-producing bacteria (Bhalla and Reinus 1998).

As shown by Stäbler et al. (1999), there is a clear connection between the amount of reduction of the bone marrow density (BMD) and the occurrence of intraosseous vacuum phenomenon. The vacuum phenomenon is indicative of osteoporotic fractures due to its high specificity (up to 100%) if plasmacytoma is excluded (Kubota et al. 2005).

Some authors described a *thin paraspinal soft tissue mass* surrounding the whole vertebral body, which could be detected in some osteoporotic vertebral body fractures. Laredo et al. (1995) described it in 41% of the osteoporotic fractures, and in 12% of the malignant fractures. It is usually less than 5–10 mm thick and shows an equal thickness all around the vertebral body, or a slight predominance around the anterior aspect of the vertebra. This paraspinal soft tissue mass may either represent a traumatic paravertebral hematoma, a post-fracture reparative process or an expression of bone marrow out of the vertebral body due to the compression forces (Laredo et al. 1995; Kubota et al. 2005), and must be differentiated from thick and focal soft tissue masses due to malignant infiltration.

Malignant fractures

The *destruction* (i.e. osteolysis) *of the anterolateral and/or posterior cortex* of the vertebral body is an extremely reliable sign of malignancy (up to 100% accuracy for destruction of the posterior cortex) (Fig. 5). It is one of most frequent CT findings in malignant compression fractures and suggests, that the destruction of the vertebral cortex is the most common trigger of vertebral body collapse in cases of malignancy (Kubota et al. 2005). CT better differentiates cortical bone comminution and burst fragments from cortical destruction than plain film radiographs, where all these findings appear as bone destruction (Sattari et al. 2008).

Laredo et al. (1995) reported in their study, that destruction of cortical bone was less common in myelomatous compression fractures than in metastatic ones. An advanced destruction of cancellous bone with relative preservation of cortical bone was considered to be a characteristic CT sign of myelomatous fractures.

Since many metastases present as soft tissue masses, destroying the vertebral structure (Moulopoulos et al.

1999), an *epidural mass* is highly specific (sensitivity 66.7%, specificity 97–100%, accuracy 85.9%) of malignant vertebral fractures (Laredo et al. 1995; Kubota et al. 2005). It usually has a convex or bilobated appearance and has to be carefully differentiated from a flatly shaped epidural soft tissue mass, sometimes appearing in osteoporotic fractures, that most likely represents epidural veins, that are displaced by the extruded bone marrow from the vertebral collapse (Sattari et al. 2008).

Metastatic paraspinal soft tissue masses in malignant fractures are typically *focal* and often involve only one part of the periphery of the vertebral body (Fig. 5). This sign is highly specific (specificity 100%) and has a sensitivity of 54.5% and an accuracy of 80.8% (Kubota et al. 2005). They are usually more than 10 mm thick and must be differentiated from the thin paraspinal masses surrounding the entire vertebral body, which are observed in osteoporotic fractures, and probably equal pressed out bone marrow or hematoma (Laredo et al. 1995).

The *destruction of a pedicle* (Fig. 5) is a highly specific finding of a malignant vertebral fracture. Metastases are frequently detected in the posterior aspects of the vertebral bodies, expanding into the posterior vertebral structures (Lecouvet et al. 1997), which can be explained by the particular blood support of the vertebral bodies (Batson 1940). Laredo et al. (1995) showed a specificity of 100% for destruction of the pedicles. The study by Kubota et al. (2005) reported similar values (sensitivity 51.5%, specificity 100%, accuracy 79.5%).

The *destruction of the cancellous bone* of the vertebral body (Fig. 5) was demonstrated as a reliable sign of malignancy (up to 97.4% accuracy) (Kubota et al. 2005). Another study by Laredo et al. (1995) showed a weak specificity (70%) for malignancy, since they observed some degree of destruction in 29% of the osteoporotic fractures, which was discussed as part of the healing response to the fracture. Probably Laredo et al. (1995) may have misinterpreted fracture lines as a destruction of cancellous bone, since they used only axial images and relatively thick slices (5 mm).

Other rather specific but not very sensitive signs of malignancy in the study by Kubota et al. (2005) are the destruction of the endplate (sensitivity 33.3%, specificity 100%, accuracy 71.8%), and a diffuse paraspinal soft tissue mass >5 mm (sensitivity 51.5%, specificity 100%, accuracy 85.9%).
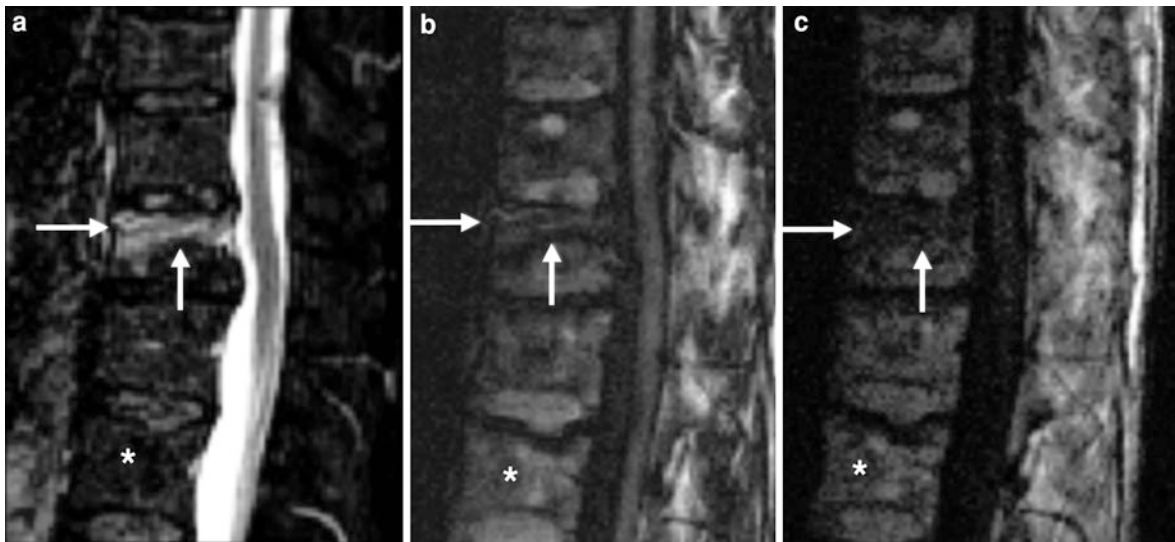
Fig. 6 75-year-old patient with a typical osteoporotic fracture and diffusion-weighted SSFP (PSIF). Sagittal STIR image (**a**) showing a strong edema (*arrows*) within the fractured L1 vertebral body. Diffusion-weighted SSFP with delta = 3 ms (**b**) showing mildly hypointense signal intensity within the edema (*arrows*) in comparison with normal vertebral marrow (*asterisk*). PSIF with delta = 6 ms (**c**) showing stronger hypointensity with higher diffusion weighting (*arrows*)

Table 1 gives an overview of the X-ray and CT features of benign and malignant vertebral fractures.

Less useful findings in differentiating benign and malignant vertebral fractures

Sclerosis, marked comminution of the cancellous bone, Schmorl's nodes and fracture of a pedicle had little or no value in the differentiation of benign from malignant vertebral fractures in the study by Laredo et al. (Laredo et al. 1995).

2.3   Magnetic Resonance Imaging

MRI is the method of choice to visualize bone marrow, while osseous structures are not well depicted due to their low proton density. Chronic benign vertebral fractures can be easily detected due to an absence of abnormal signal intensity on STIR and T1w images in the compressed vertebra (An et al. 1995; Jung et al. 2003). The distinction between metastatic and acute osteoporotic vertebral fractures on the basis of MR imaging findings has a sensitivity of 85–100%, a specificity of 79–100%, and an accuracy of 86–95%, depending on the patient population (Frager et al. 1988; An et al. 1995; Shih et al. 1999; Jung et al. 2003).

Osteoporotic fractures

In osteoporotic compression fractures the *vertebral body* appears *hypointense on T1-w images* and *hyperintense on fat saturated sequences such as STIR* (Yuh et al. 1989; Baker et al. 1990; Cuenod et al. 1996; Leeds et al. 2000). *T2-w images* show a *normal or heterogeneously to homogenously abnormal signal*, which may be *related to the age* of the fracture (Yuh et al. 1989). Areas corresponding to the *fracture line* or *trabecular impaction* can be seen on *T2-w images* as linear regions with low signal (Uetani et al. 2004). The acute signal abnormalities are *mostly incomplete or band-like* (Yuh et al. 1989; Baker et al. 1990; Cuenod et al. 1996; Baur et al. 1998, 2002b) (Fig. 6a) and appear well-defined in about 71% and ill-defined in about 29% of the cases (Shih et al. 1999). Figure 7 shows a typical acute and typical old osteoporotic fracture.

Contrast-enhanced T1-w images show a complete or partial equalization of the signal intensity in comparison with normal, not fractured vertebrae, termed "*return to normal signal intensity*" (Cuenod et al. 1996). Acute cases of osteoporotic collapse may show an intense contrast-enhancement (Cuenod et al. 1996). Subacute or chronic benign fractures show a slight enhancement that can either be homogenous or heterogeneous with

Fig. 7 66-year-old patient with a typical acute osteoporotic fracture in L4 (*asterisk*) and a typical old osteoporotic fracture in Th 12 (*arrow*). **a** STIR image showing a high signal intensity in the acute fracture in L4 and an isointense signal intensity in the old fracture in Th 12. The acute fracture (*asterisk*) shows a high signal intensity area in the T2-w image (**b**) and a low signal intensity in the T1-w image without fat-saturation (**c**) due to edema. The healed fracture (*arrow*) shows a high signal intensity in the T2-w (**b**) and in the T1-w image without fat-saturation (**c**) due to fatty replacement

greater enhancement in the posterior vertebral body, which might be due to blood stasis as a result of fracture (Shih et al. 1999). Accordingly, contrast-enhancement in the vertebral body is no reliable sign to distinguish benign and malignant vertebral fractures until edema has been absorbed.

On T1-w images most benign fractures show some amount of normal fatty marrow that is opposite to the fractured endplate. The *band-like hypointense region adjacent to the preserved marrow* is considered specific for osteoporotic collapse (An et al. 1995; Cuenod et al. 1996; Moulopoulos et al. 1996). Fibrotic replacement of bone and marrow after a fracture can cause temporary hypointensity on T1-w images and might be mistaken for malignancy (Vaccaro et al. 1999). Nineteen percent of cases of benign collapse show focal areas of signal abnormality in other adjacent vertebrae that often corresponds to benign fracture lines, bone impaction or Schmorl's nodes, but cannot always be differentiated from metastasis with T1-w imaging alone (Cuenod et al. 1996). Osteoporotic fractures without remaining fatty marrow and a resulting complete vertebral body involvement can easily be confused with malignant fractures (Fig. 10) (Moulopoulos et al. 1996; Baur et al. 1998). Histology in osteoporotic vertebral compression fractures shows

Fig. 8 75-year-old patient with an acute osteoporotic fracture of L2. Sagittal CT (**a**) showing a retropulsion of a bony fragment into the spinal canal (*arrow*). Also the both caudal vertebral bodies are fractured. There is also a small vacuum sign adjacent to the fractured vertebral cover plate (*arrowhead*). Corresponding sagittal STIR (**b**), T2-w (**c**) and T1-w (**d**) images
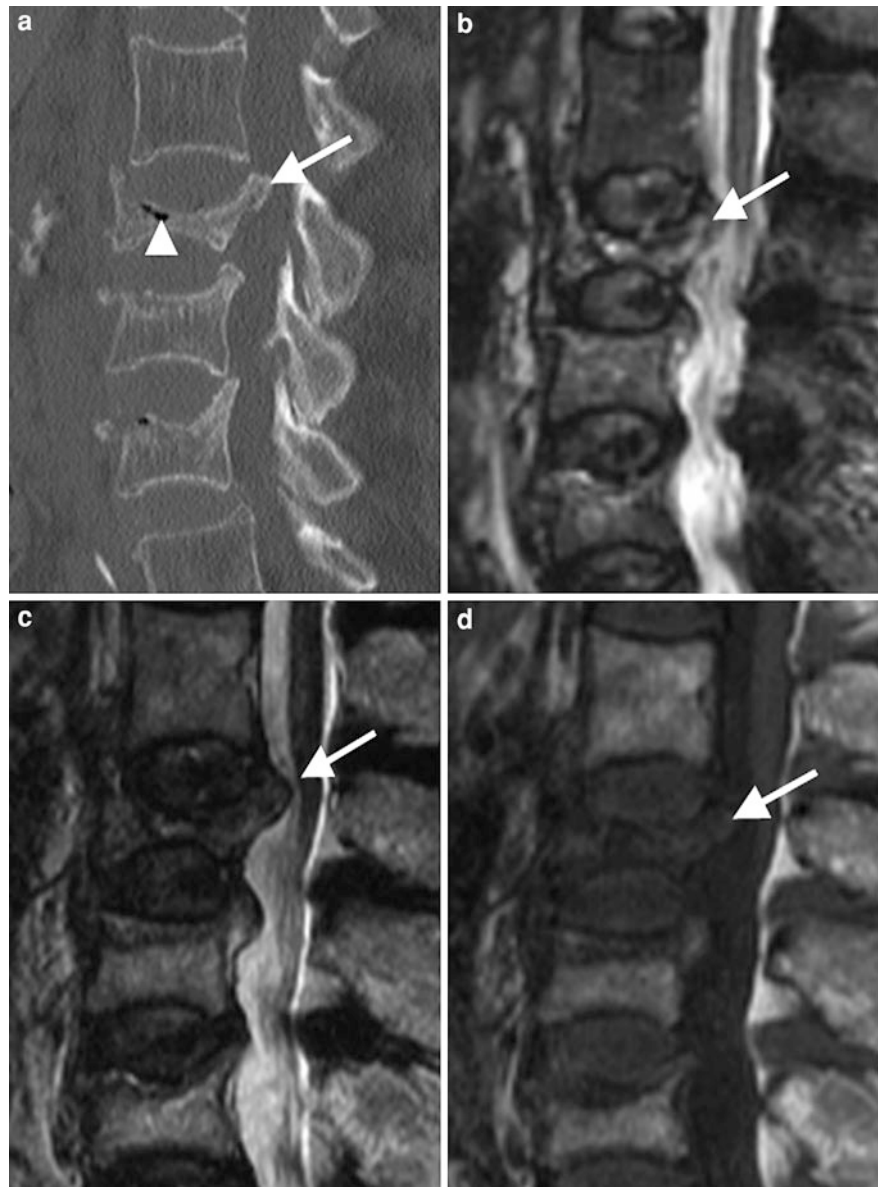
bone marrow edema, fibrosis, increased trabecular turnover, and hemorrhage.

The size of the altered signal remains unchanged in the initial 2–4 months and then gradually reverts to normal. The time to complete restoration of the normal marrow signal intensity is variable (3–6 months) (Yuh et al. 1989; Cuenod et al. 1996), but usually does not exceed 12 months. Healed fractures usually show again hyperintense signal on T1-w SE and hypointense signal on fat suppressed images, such as STIR, and do not enhance with contrast (Fig. 7). Often the fat signal is even higher than in the

neighboring vertebral bodies due to a higher amount of fat cells within the healed vertebral body.

The *retropulsion of a posterior or posterosuperior bone fragment* of the vertebral body into the spinal canal (Fig. 8) is highly specific of an osteoporotic fracture (specificity 89–100%), but an intermediate to low sensitivity (16–60%) has been reported (Tan et al. 1991; Cuenod et al. 1996; Jung et al. 2003). One study (Tan et al. 1991) showed this finding only in osteoporotic fractures. Another study found retropulsion of bony fragments in both osteoporotic and malignant vertebral fractures, but significantly

associated with osteoporotic fractures (Jung et al. 2003). Usually the retropulsed fragment does not lead to a significant spinal stenosis (Cuenod et al. 1996).

Multiple compression fractures are a rather weak sign of osteoporotic fractures, since they are also typical in multiple myeloma. In a study on 55 acute osteoporotic and 27 malignant vertebral compression fractures, Jung et al. (2003) found a significant correlation of multiple compression fractures with non-malignancy. However this is not a reliable sign. In patients with myeloma a mixture of signs may be present. Myeloma patients may show the typical focal soft-tissue lesion within a vertebral body, leading to a fracture due to osteolysis. On the other hand, some patients have diffuse disease, leading to diffuse osteoporosis and thus multiple vertebral fractures. Under these circumstances the amount of tumor cells may be limited. Therefore the fractures do not show the typical signs of a pathologic fracture (Lecouvet et al. 1997). In addition to that, myeloma patients are usually elderly subjects with preexisting osteoporosis which can by itself lead to osseous weakening and therefore to an osteoporotic fracture. Rupp et al. (1995) performed a study on 18 malignant and 16 osteoporotic vertebral compression fractures including patients with multiple myeloma, and did not find any significant difference between osteoporotic and malignant vertebral compression fractures.

The *fluid sign* is defined as a focal, linear, or triangular area of strong ("fluid-like") hyperintensity on STIR images on a background of diffuse hyperintensity in the vertebral body because of acute collapse (Fig. 4). The signal intensity of the fluid sign has to be equivalent to that of cerebrospinal fluid. In a former study (Baur et al. 2002b), we showed, that the fluid sign is significantly associated with osteoporotic vertebral fractures, while rarely seen in malignant fractures. Osteoporotic fractures show a significant correlation of the fluid sign with the severity of the fracture. The fluid sign corresponded to osteonecrosis, edema, and fibrosis in histological examination.

Malignant fractures

Spin-echo T1-w images mostly show a *complete replacement of normal bone marrow* with *diffuse hypointense signal in the whole vertebral body* (Cuenod et al. 1996). *Spin-echo T2-w images* show an *isointense to hyperintense signal* with a homogeneous (Baker et al. 1990) or heterogeneous (Cuenod et al. 1996) pattern. After intravenous administration of *gadolinium-containing contrast agent*, the signal is *hyperintense on T1-w fat suppressed images* compared to surrounding normal marrow (Leeds et al. 2000) with mostly heterogeneous enhancement due to uneven blood supply or tumor necrosis (Shih et al. 1999). However, up to 33% of the cases show incomplete marrow replacement with small areas of preserved fatty marrow. Usually the marrow replacement in malignant fractures is circumscribed and focal, whereas in osteoporotic fractures it is band-like or diffuse (Yuh et al. 1989; Cuenod et al. 1996). Figure 9 shows a malignant vertebral fracture due to breast cancer.

The signal changes of malignant fractures commonly progress or persist and do not show a return to normal signal, because tumor persists without restoration of normal fatty bone marrow.

Most malignant compression fractures do not only show *involvement* of the bone marrow of the vertebral body, but also of the *pedicles and the neural arch*. Involvement of the pedicles has a sensitivity of 80%, a specificity of 94%, a positive predictive value of 86% and a negative predictive value of 91% for a malignant fracture (Cuenod et al. 1996). In the cases with pedicle involvement, there is a complete affection in 75% and an incomplete affection in 25% (Moulopoulos et al. 1996). About 55% of the cases with pedicle involvement show an expansion of the pedicles (Shih et al. 1999). However abnormal signal intensity in pedicles can also be observed on contrast-enhanced T1-w images with fat suppression or on STIR images due to extension of the edema into the pedicle in up to 9% of the cases in osteoporotic fractures (Kaplan et al. 1987; Yuh et al. 1989; Jung et al. 2003). Additional CT can help excluding a fracture of the pedicles that may be responsible for the signal changes. Ishiyama et al. (Ishiyama et al. 2010) found frequent pedicle involvement in the early phase of osteoporotic compression fractures and suggested, that the diagnosis of a malignant fracture should not be assumed when pedicle involvement is the only present sign (Fig. 10).

Epidural soft-tissue masses are, if present, a highly specific sign for malignant vertebral collapse (Fig. 9e), especially when it is an encasing epidural mass (Tan et al. 1991; Jung et al. 2003). The tumor tissue spreads out of the vertebral body and grows into the spinal canal. The specificity of this sign for a malignant vertebral fracture is up to 100%, and its sensitivity is 80% (Cuenod et al. 1996).

Fig. 9 64-year-old patient with a typical malignant fracture of Th 3 due to breast cancer. **a** CT in bone window showing a mainly sclerotic metastasis in the fractured vertebra and a posterior bulging (*arrow*); **b** sagittal STIR image showing a hyperintense signal in the whole fractured vertebral body (*asterisk*), a posterior bulging (*arrow*) and another metastasis (*arrowhead*) in an adjacent vertebral body; **c** corresponding T2-w image showing hypointense signal in the whole fractured vertebral body due to the mainly sclerotic nature of the metastases (*asterisk*). The spinal canal is narrowed (*arrow*). Sagittal T1-w images before (**d**) and after (**e**) i.v. administration of Gadolinium-containing contrast agent showing enhancement in the fractured vertebral body (*asterisk*) and the further metastasis in Th 2 (*arrowhead*). Please also note the contrast enhancing epidural tumor mass (*arrow*) in (**e**)

Focal paraspinal masses caused by tumor growth are, if present, typical for metastatic compression fractures and have a sensitivity of 41%, a specificity of 93% and an accuracy of 75% (Jung et al. 2003).

In malignant compression fractures, the underlying tumor leads to an expansion of the vertebral body which results in a *convex bulge involving the whole posterior cortex* (Fig. 9). This sign has a sensitivity of 70–74%, a specificity of 80–94%, a positive predictive value of 84%, a negative predictive value of 87% and an accuracy of up to 78% (Cuenod et al. 1996; Jung et al. 2003). However, it is also seen in 2–19% of osteoporotic fractures, probably caused by bone marrow pushed out during the collapse (Rupp et al. 1995; Cuenod et al. 1996; Moulopoulos et al. 1996).

Table 2 *MRI features* of benign and malignant vertebral fractures

Benign osteoporotic fracture	Malignant fracture
Spared normal bone marrow, incomplete or band-like signal changes	Complete replacement of normal vertebral bone marrow, diffuse hyperintense signal on STIR
Isointensity after Gd on T1w images ("*return to normal signal intensity*")	High/inhomogenous SI after Gd on T1w images
No involvement of the pedicles and the neural arch	Involvement of the pedicles and the neural arch
Intravertebral "*fluid sign*"	No intravertebral "*fluid sign*"
No or only thin surrounding paraspinal mass	Epidural soft tissue mass—focal paraspinal mass
Retropulsion of posterior bone fragment into spinal canal	Bulging of posterior cortex
Other (old) osteoporotic fractures	Other spinal metastases

Frequently well-demarcated round signal abnormalities in the marrow of other than the collapsed vertebrae can be found, indicating *other spinal metastases* (Fig. 5) (Cuenod et al. 1996; Jung et al. 2003).

Table 2 gives an overview of the MRI features of benign and malignant vertebral fractures.

The described morphological features may help in the differentiation of benign and malignant fractures in most of the cases, but especially in acute (Tan et al. 1991) and subacute (Frager et al. 1988) fractures, unequivocal results can lead to a wrong diagnosis. Correlation with other imaging techniques like CT, follow-up imaging or, in selected cases, bioptic samples may help in making the correct diagnosis. CT provides information on the osseous structures, that cannot reliably be depicted by MRI, and often shows destruction of the cortical bone, cancellous bone, and pedicle in malignant fractures, as mentioned before (Laredo et al. 1995).

Since vertebral fractures due to multiple myeloma often have the appearance of benign osteoporotic fractures on MRI (Lecouvet et al. 1997), they should be taken in consideration in cases of non-traumatic, benign-appearing vertebral compression fracture (Uetani et al. 2004).

New MR imaging techniques of bone marrow like diffusion-weighted imaging (DWI), perfusion imaging and chemical-shift imaging, as well as PET-CT techniques can provide additional information, which may help in differentiating acute benign and malignant vertebral fractures in cases where morphological CT and MRI signs are insufficient in the determination of fracture etiology. These emerging techniques are discussed in the following chapters.

3 Advanced Techniques for the Differentiation of Benign and Malignant Vertebral Fractures

3.1 Diffusion-Weighted Imaging

Conventional MRI is very sensitive but not always specific in the differentiation of acute osteoporotic and malignant vertebral fractures. Several studies suggested that diffusion-weighted MR imaging (DW-MRI) could be useful to distinguish between benign and malignant vertebral compression fractures (Baur et al. 1998; Park et al. 2004; Thurnher and Bammer 2006; Oztekin et al. 2009).

There are two ways to assess vertebral fractures with DWI-MRI. On one hand, the signal intensity of diseased vertebrae can be compared with normal appearing vertebrae and can be qualitatively characterized as hypo-, iso- or hyper-intense. On the other hand, quantitative imaging uses the apparent diffusion coefficient (ADC) that is calculated using two or more images with different diffusion weightings (b-values). These ADC values can be used to characterize the lesions quantitatively.

Acute osteoporotic fractures show an increased diffusion with low signal intensity on diffusion-weighted scans and high values on ADC maps, which is explained by the disruption of the trabecular structure and bone marrow edema in the diseased vertebrae.

Malignant fractures tend to be associated with restricted diffusion, i.e. high signal intensity on diffusion-weighted scans and lower values on ADC maps. In spinal tumors with vertebral body compression
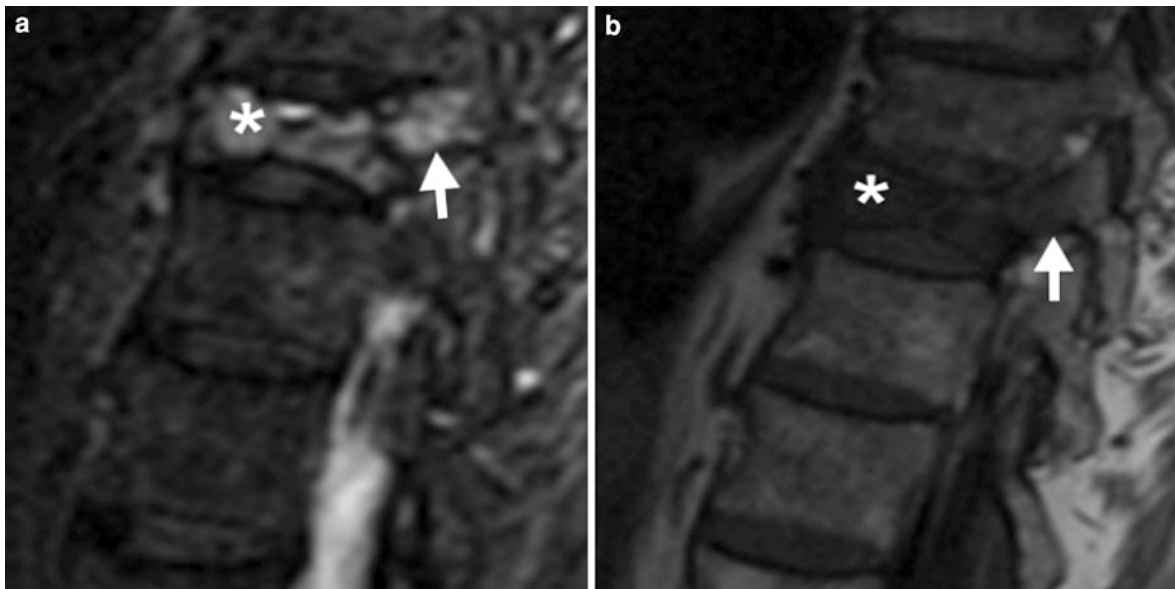
Fig. 10 68-year-old patient with a typical osteoporotic fracture of L2. The sagittal STIR image (**a**) shows a high signal intensity in the pedicle (*arrow*). The sagittal T1-w image (**b**) shows a low signal intensity in the pedicle (*arrow*). Signal changes in the whole vertebral body (*asterisk*) plus involvement of the pedicles are usually signs of malignancy, but can also be observed in osteoporotic fractures due to extension of edema or fracture in the pedicles

fractures, increased tumor cell packing leads to a smaller and more restricted extracellular space, resulting in increased signal from restricted water protons, as has been observed in lytic metastases (Baur et al. 2003).

The reverse fast imaging with steady-state free-precession (PSIF) sequence is a diffusion-weighted steady-state free-precession (SSFP) sequence, where only a single (monopolar) diffusion gradient is inserted into each repetition time (TR). The exact quantification of ADC is not possible with this sequence, due to the influence of many different parameters (Dietrich et al. 2009). In a first study (Baur et al. 1998), we evaluated the usefulness of the PSIF sequence in the differentiation of 22 acute benign and 39 acute malignant vertebral body fractures, and showed that all benign vertebral compression fractures were iso- or hypo-intense, while malignant fractures were hyper-intense in comparison with normal adjacent vertebral bodies. In another own study (Baur et al. 2002a), we examined a larger group of patients, where hyperintensity as a sign of malignancy in a vertebral fracture on PSIF provided a sensitivity of 100%, a specificity of 93%, a positive predictive value of 91% and a negative predictive value of 100%. The PSIF sequence is relatively fast and insensitive to bulk motion. Using a diffusion-weighted SSFP sequence, the differences between benign and malignant vertebral body fractures are clearer than when using alternative pulse sequences like single-shot EPI, single-shot TSE, or conventional spin-echo or stimulated-echo sequences (Dietrich et al. 2009). Figures 6 and 11 show an osteoporotic and a malignant vertebral fracture on STIR and diffusion-weighted SSFP sequences (PSIF).

Hypointense vertebral metastases in diffusion-weighted SSFP (Castillo et al. 2000) may be explained by former treatment with radiotherapy or sclerosis with lower water content (Dietrich et al. 2009). Sclerotic vertebral metastases of prostate cancer show less signal than metastases of other tumors (Hacklander et al. 2006). In a meta-analysis of eight studies, it could be shown, that lesions classified as "hypointense" or "hypointense and isointense" were significantly more likely to be benign (Karchevsky et al. 2008).

Using PSIF with a diffusion-pulse length of 3 ms provides the best differentiation of benign and malignant fractures. In unclear cases, an additional diffusion-pulse with a length of 6 ms can be applied, where osteoporotic fractures become hypointense, while malignant fractures remain hyperintense (Baur et al. 2001, 2002a). Because the contrast to
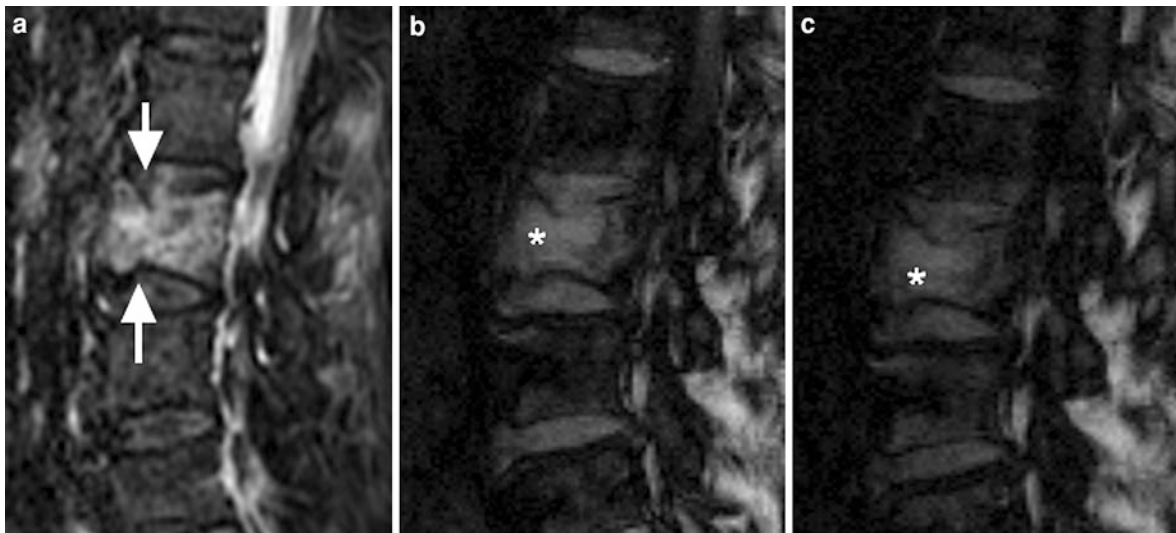
Fig. 11 71-year-old patient with a malignant fracture of L3 due to metastasis of adenocarcinoma and diffusion-weighted SSFP (PSIF). Sagittal STIR image (**a**) showing edema in the whole vertebral body and end plate fractures. Diffusion-weighted SSFP with delta = 3 ms (**b**) and delta = 6 ms (**c**) showing a hyperintense signal intensity in the edema (*asterisk*) in comparison with normal vertebral marrow

normal bone marrow is used, patients with known hematologic disorders like osteomyelofibrosis or leukemia should not be evaluated with a PSIF sequence (Baur et al. 2002a).

Figures 6 and 11 show a typical osteoporotic and a typical malignant vertebral fracture on STIR and diffusion-weighted SSFP sequences (PSIF).

Another imaging technique, echo-planar imaging (EPI), decreases acquisition time, but general problems of this technique are a limited spatial resolution, sensitivity to eddy currents and local susceptibility gradients, as well as chemical-shift (Le Bihan 1998). Oztekin et al. (2009) used diffusion-weighted EPI with a b-value of 300 s/mm^2 and examined patients with osteoporotic and traumatic vertebral fractures and vertebral tumor infiltration. A hyperintense signal was highly sensitive and specific for metastatic tumor infiltration (93% sensitivity, 90% specificity). Sclerotic metastases were found to be hypointense.

Tang et al. (2007) examined the influence of the b-value in the differentiation of benign and malignant vertebral compression fractures using EPI with spectral presaturation and inversion recovery (SPIR) and b-values of 0–800 s/mm^2. They found that b-values around 300 s/mm^2 provided the best differentiation between benign and malignant fractures. All malignant fractures were hyperintense, while most benign fractures were isointense and a few slightly hyperintense at this b-value.

Park et al. (2004) used a diffusion-weighted single-shot fast spin-echo sequence with a b-value of 500 s/mm^2. In this study, all benign fractures had low signal intensities on diffusion-weighted images. Malignant vertebral tumors showed a heterogeneous signal behavior with hypointensity in 58%, intermediate signal intensity in 25%, and hyperintensity in 6%. With a high or intermediate signal intensity indicating malignancy, the study found a high specificity of 95% but a low sensitivity of 42%. The authors concluded that the differences in the malignant lesions were due to patient selection bias and different degrees of T2 shine through effect.

The differences in the signal behavior in the studies mentioned above may be explained by the different diffusion weightings, the different sequence types and sequence parameters. At low b-values <150 s/mm^2, the diffusion effect can be overestimated due to the contribution of perfusion and T2 shine through effect (Chan et al. 2002; Herneth et al. 2005), while high b-values >600 s/mm^2 may lead to an underestimation due to signal intensities comparable with the noise level (Dietrich et al. 2009).

Several studies applied quantitative DWI to normal and pathological vertebral bone marrow. Although the results showed a certain variability, the majority of the studies revealed typical ADC ranges associated with normal and pathological bone marrow. Normal bone

marrow shows ADCs of 0.2–0.5×10^{-3} mm^2/s. Metastases or malignant fractures range from ~ 0.7 to 1.0×10^{-3} mm^2/s, osteoporotic or traumatic fractures show ADCs of ~ 1.0–2.0×10^{-3} mm^2/s (Dietrich et al. 2009). Studies always showed a remarkable overlap, which limited the value of quantitative DWI in differentiating between benign and malignant fractures. Figures 12 and 13 show the ADC maps of a malignant and an osteoporotic fracture.

The calculation of ADC values eliminates the influence of the T2 weighting and depicts the cellular barriers in the tissue, but low signal-to-noise-ratio in diffusion-weighted fast spin-echo sequences is a major source of error, that leads to an overlap and diminishes accuracy (Zhou et al. 2002). The most important influence is the application of fat saturation, which is required for single-shot EPI but is optional in combination with SE or FSE techniques. Because the ADC of vertebral fat is close to zero, the ADCs of normal bone are systematically decreased, when fat saturation is not applied (Dietrich et al. 2009).

Using a fast spin-echo diffusion-pulse sequence with b-values of 0–250 s/mm^2, Zhou et al. (2002) showed, that metastatic vertebral fractures show ADC values of 1.9×10^{-4} mm^2/s $\pm\ 0.3 \times 10^{-4}$ mm^2/s and benign fractures show ADC values of 3.2×10^{-4} mm^2/s $\pm\ 0.5 \times 10^{-4}$ mm^2/s with significant differences between both groups, but with a substantial overlap. Lesions were better separated on the basis of ADC values than on conventional T1-w, T2-w, contrast-enhanced T1-w or qualitative diffusion-weighted images. Sensitivity, specificity, and accuracy were not reported.

Biffar et al. (2010a) examined 24 osteoporotic vertebral fractures and 20 malignant vertebral fractures and showed, that DW-ssTSE (b-values 100, 250, 400, 600 s/mm^2) could significantly discriminate between both entities showing a sensitivity of 65% and specificity of 88% at an ADC of 1.49×10^{-3} mm^2/s as a cutoff-value. DW-EPI showed no statistical differences due to an underestimated signal attenuation and gross geometrical image distortions caused by susceptibility heterogeneities.

Chan et al. (2002) examined 25 acute osteoporotic fractures in 18 patients, 18 acute malignant fractures in 12 patients and 6 acute fractures due to tuberculosis in 2 patients, with a diffusion-weighted EPI sequence at 1.5 T. ADC values were calculated, using b-values of 200, 500, 800, and 1,000 s/mm^2. The quantitative evaluation showed mean ADC values of 0.82×10^{-3} mm^2/s for malignant fractures, and 1.92×10^{-3} mm^2/s for osteoporotic fractures, revealing a significant difference between these two entities ($p < 0.001$). Fractures due to tuberculosis (mean ADC 0.98×10^{-3} mm^2/s) were not significantly different from malignant fractures. Additionally, the signal intensities of the collapsed vertebral bodies were qualitatively assessed at a b-value of 1,000 s/mm^2, where all benign acute vertebral fractures were hypointense. The malignant fractures were hyperintense, except sclerotic metastases, which were hypointense and showed ADC values close to zero.

In a meta-analysis Karchevsky et al. (2008) reviewed 4 studies assessing the ADC values of benign and malignant vertebral fractures and showed, that mean ADC values in benign fractures were significantly higher than malignant fractures with a standardized mean difference (SMD) of 2, 8 and a 95% confidence interval for the SMD of 2.1 to 3.5. Mean ADCs of pathologic fractures and malignant lesions were in the range from 0.19 to 0.853×10^{-3} mm^2/s, benign fractures showed ADCs from 0.32 to 1.94×10^{-3} mm^2/s.

The ADC value shows significant differences between benign and malignant vertebral fractures, but all studies showed a remarkable overlap limiting its specificity. Although the ADC value itself should be independent from sequence type and sequence parameters, the measured values are influenced by sequence specific artifacts, range of used b-values, application of fat saturation, noise, and perfusion effects. DWI of bone marrow requires considerably more robust imaging techniques than typical MRI of the brain. Being still a technique undergoing active research, DWI of the bone marrow provides a unique imaging method, which can help in the differentiation of benign and malignant vertebral fractures.

3.2 In-Phase/Opposed-Phase (Chemical-Shift) Imaging

In-phase (IP)/opposed-phase (OP) imaging (also known as chemical-shift imaging) uses the different precession frequencies of water and fat protons due to the differences in their molecular environment. Water and fat protons are in-phase with one another at a TE of 4.6 ms, and 180° opposed at a TE of 2.3 ms at
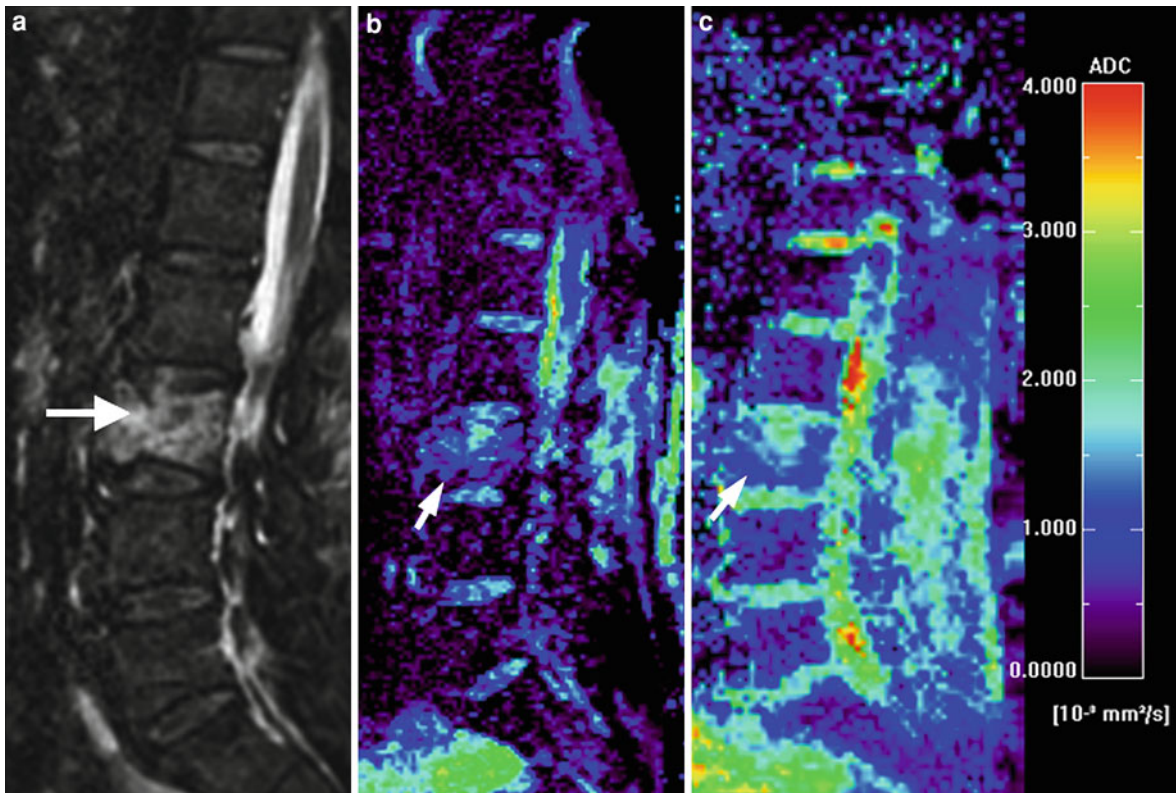
Fig. 12 71-year-old patient with a malignant fracture of L3 due to metastasis of adenocarcinoma and DWI. Sagittal STIR image (**a**) showing hyperintense signal in the whole diseased vertebral body. ADC maps calculated from DW-EPI (**b**) and DW-HASTE (**c**) images showing average ADC values of 0.9×10^{-4} mm²/s (DW-EPI) and 1.38×10^{-4} mm²/s (DW-HASTE) (*arrows*)

1.5 T. When there are both fat and water protons in a given voxel, there will be some signal intensity loss on images that are obtained, when the protons are in their opposed-phase, without a refocusing pulse. More signal intensity loss occurs when the volume of fat and water is roughly equal (Erly et al. 2006). The percentage decrease of the bone marrow signal intensity on opposed-phase images compared with in-phase images (Zajick et al. 2005) or the relative signal intensity ratio (signal intensity$_{OP}$/signal intensity$_{IP}$) (Eito et al. 2004; Erly et al. 2006) can be calculated for quantitative measurement.

Normal vertebral bone marrow has fat and water components. In adults, the vertebrae, sternum, and ribs contain hematopoietic red marrow, which has about 40% fat content while yellow marrow contains 80% fat (Eastell 2007). Malignant neoplasms tend to replace the fatty marrow components and therefore cause a lack of suppression on the opposed-phase

images. Benign vertebral fractures usually show no marrow displacement, which results in low signal intensity on the opposed-phase images (Baker et al. 1990; Eito et al. 2004; Zajick et al. 2005; Erly et al. 2006). Figures 14 and 15 show the IP and OP images and the calculated ratios of an osteoporotic and a malignant vertebral fracture.

If vertebral bodies are highly deformed and compressed, containing almost no water or fat, they may show weak signal intensity in OP and IP images, resulting in a high signal intensity ratio mimicking malignancy. Therefore, signal intensity ratios may be high because the decreased signal intensity is related to decay resulting from the use of TEs of 2.3 to 4.6 ms. T1-w images can be used to show a signal loss due to severe compression (Eito et al. 2004). One study noticed the return of a malignant lesion to a benign signal intensity ratio after treatment with X-ray therapy, whereas the standard spin-echo
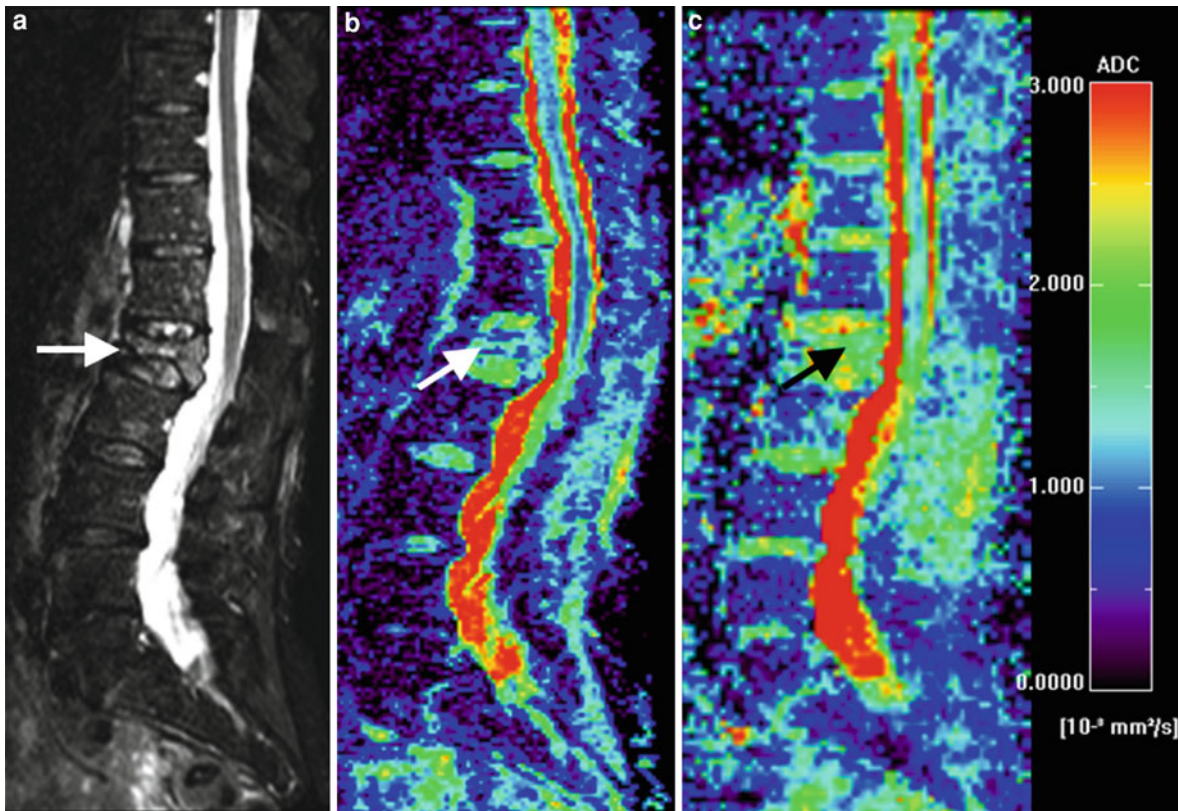
Fig. 13 70-year-old patient with an osteoporotic fracture of L2 and DWI. Sagittal STIR image (**a**) showing hyperintense signal in the whole fractured vertebral body. ADC maps calculated from DW-EPI (**b**) and DW-HASTE (**c**) images showing higher (compared with malignant fractures) average ADC values of 1.25×10^{-4} mm^2/s (DW-EPI) and 1.73×10^{-4} mm^2/s (DW-HASTE) (*arrows*)

sequences remained abnormal, suggesting that in-phase/opposed-phase imaging might be an early marker for response to treatment of osseous metastatic disease, but studies on this are still lacking (Erly et al. 2006).

Eito et al. (2004) showed, that at 1.5 T normal non-fractured vertebrae have mean signal intensity ratios of 0.46 ± 0.14 (SD), whereas non-neoplastic fractured vertebrae (mean 0.63 ± 0.21 SD) and malignant compression-fractured vertebrae (mean 1.02 ± 0.11 SD) have higher signal intensity ratios (i.e. the signal drop from in-phase to opposed-phase is highest in normal vertebrae, whereas non-malignant fractures and malignant fractures show less signal drop or even increased signal intensity on opposed-phase images). All three groups showed significant differences between each other.

Erly et al. (2006) compared 29 benign compression fractures and 20 malignant lesions at 1.5 T, and showed a significant difference of the mean signal intensity rates of benign vertebral compression fractures (0.58 ± 0.02 SD) and malignant vertebral compression fractures (0.98 ± 0.095 SD). Performing ROC-analysis, a signal intensity ratio of >0.8 indicating malignancy showed best discrimination of benign and malignant vertebral fractures with a sensitivity of 95% and a specificity of 89%.

Zajick et al. (2005) examined normal vertebral bone marrow, benign lesions, and metastases. They found a decrease in signal intensity for all normal vertebrae (mean 58.5%) and for benign lesions (endplate degeneration mean 52.2%, Schmorl's nodes mean 58.0%, hemangiomas mean 49.4%, benign fractures 49.3%) on opposed-phase images. Metastases showed either a minimal decrease or an increase of signal intensity (mean 2.8% decrease). Although the results showed overlaps between the different groups, the authors suggested a decrease in signal
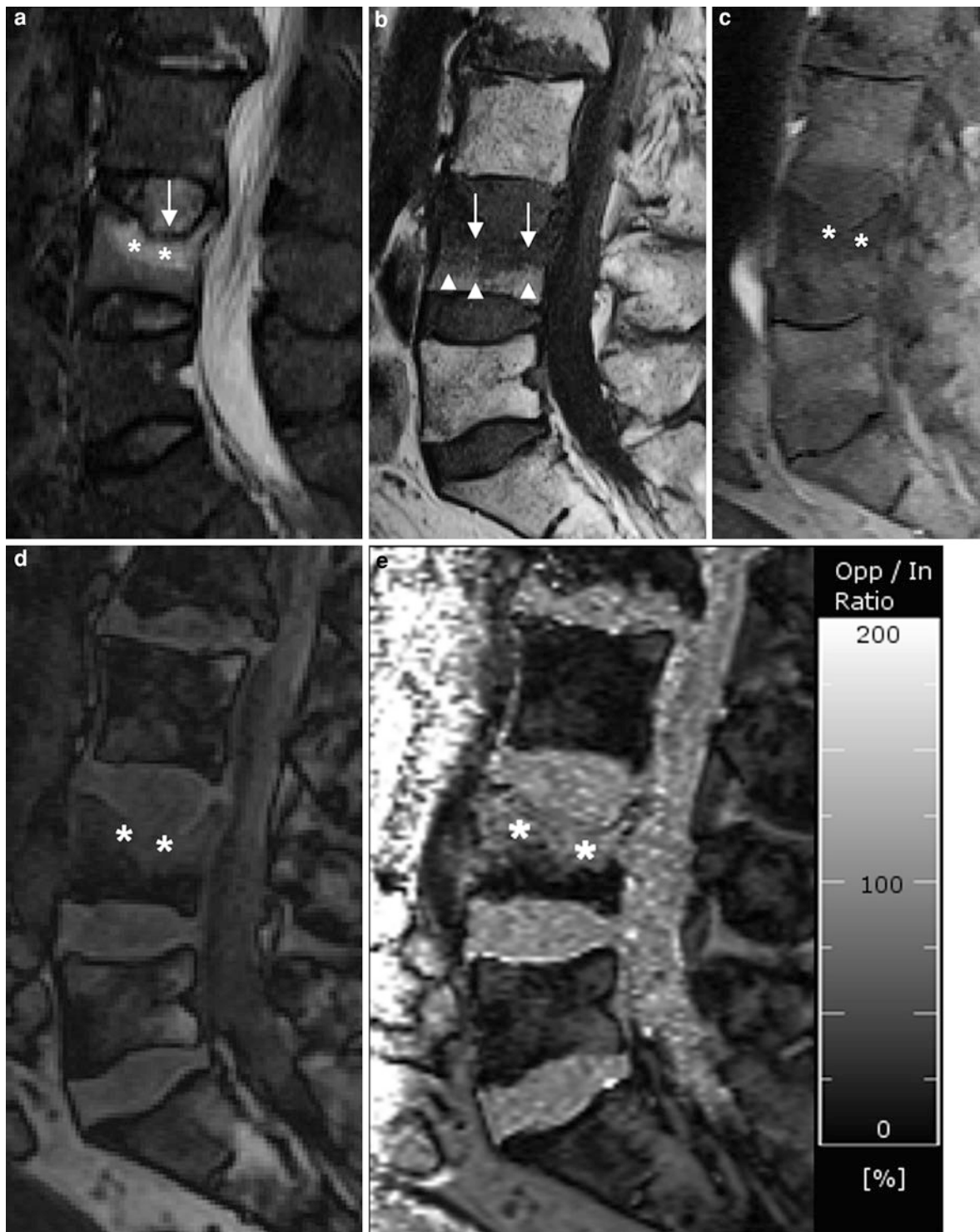
Fig. 14 67-year-old patient with an osteoporotic fracture of L4 and chemical-shift imaging. STIR image (**a**) showing a band-like edema (*asterisks*) adjacent to the impressed upper vertebral end-plate (*arrow*). T1-w image (**b**) showing the hypointense signal of the edema (*arrows*) and the preserved fatty marrow adjacent to the opposite cover plate (*arrowheads*). Corresponding in-phase (**c**) and opposed-phase (**d**) images showing a signal drop on the opposed-phase image. A map showing the calculated opposed-phase/in-phase ratio (**e**) exhibits a signal drop of 39% corresponding to an opposed-phase/in-phase ratio of 61% in the edema (*asterisks*). Normal fatty marrow shows a greater signal drop due to the almost equal amount of fat and water bound protons in normal marrow

Fig. 15 60-year-old patient with a malignant fracture of L3 due to metastasis of hypopharyngeal carcinoma. Sagittal STIR image (**a**) showing hyperintense signal in the whole diseased vertebral body (*arrow*). T1-w image (**b**) showing hypointense signal (*arrow*). Corresponding in-phase (**c**) and opposed-phase (**d**) images showing a slight signal drop on the opposed-phase image (*arrow*), while normal vertebral bodies (*asterisk*) show a great signal drop. A map showing the calculated opposed-phase/in-phase ratio (**e**) exhibits a signal drop of 9% corresponding to an opposed-phase/in-phase ratio of 91% in the edema pattern (*arrow*). Normal fatty marrow (*asterisk*) shows a greater signal drop due to the almost equal amount of fat and water bound protons in normal marrow
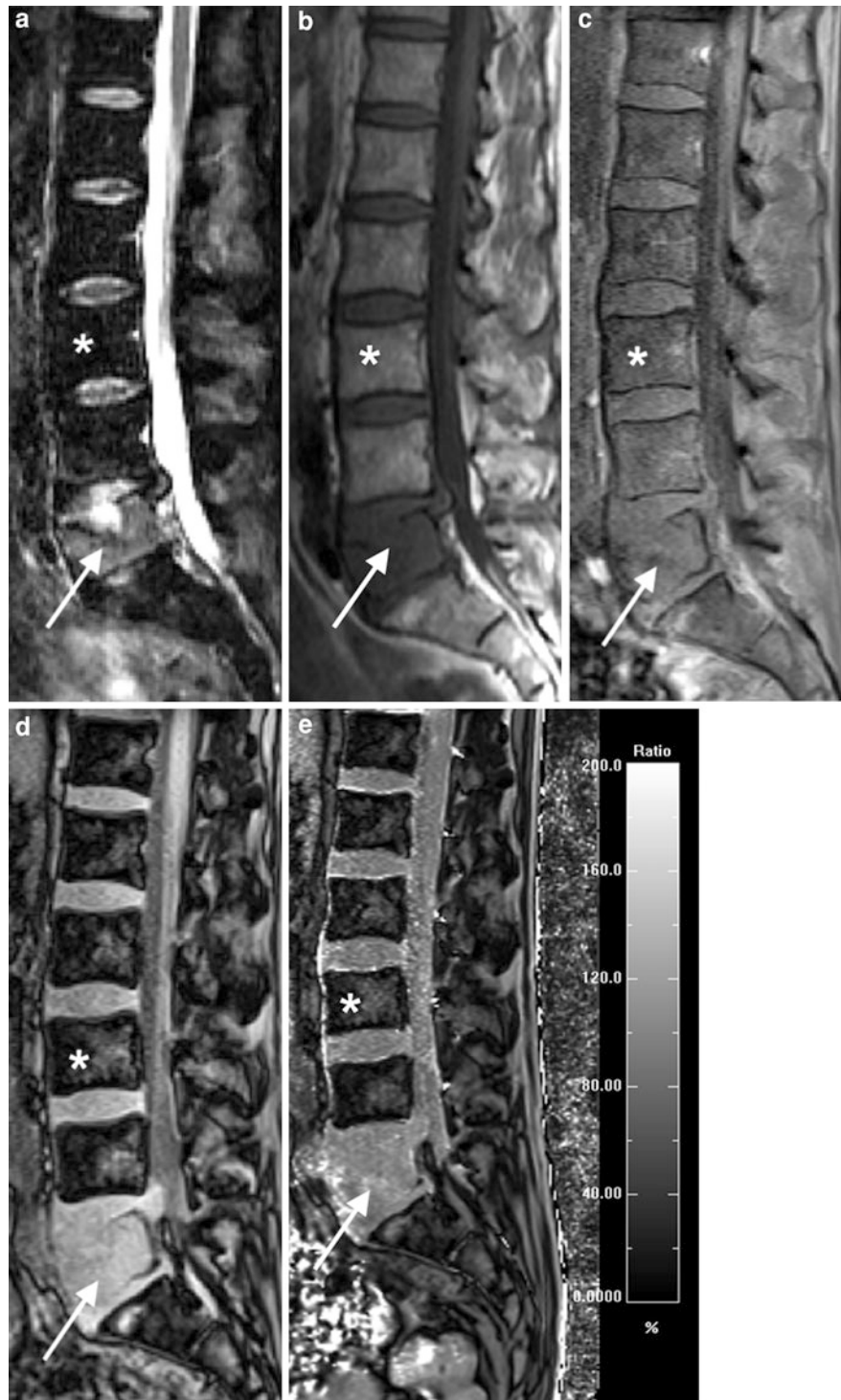
intensity of more than 20% on opposed-phase images compared with in-phase images to be a reliable cut-off threshold for benign vertebral bone marrow abnormalities, while malignant vertebral bone marrow lesions show less than 20% decrease in signal intensity.

Ragab et al. (2009) examined patients with osteoporotic and neoplastic vertebral fractures and showed a different proportional change (percentage decrease) of marrow signal intensity in OP compared with IP of 58.51 ± 9.38 for osteoporotic and 13.55 ± 11.63 for neoplastic lesions. A decrease in SI >35% as a cut-off value showed a sensitivity of 95% and a specificity of 100% with a positive predictive value of 100% and a negative predictive value of 95.2%.

Thus in-phase/opposed-phase imaging is a reliable additional tool for the differentiation of benign and malignant vertebral collapse. However, if strong edema and reduced fat content are present, the signal intensities can also be high on opposed-phase images in osteoporotic fractures. Care should be taken to acquire the same sequence type with the appropriate sequence parameters, since a slight shift e.g. in TE and flip-angle can cause a significant shift in contrast.

3.3   Dynamic Contrast-Enhanced MRI

Dynamic contrast-enhanced (DCE)-MRI does not focus on morphological features but uses measurements of the signal changes of intravenously administered contrast agents over time to measure hemodynamic parameters, using ultra-fast imaging methods. Gadolinium-containing contrast agents show similar pharmacokinetics to that of iodinized contrast agents and produce an increase of signal intensity (SI) in T1-w images by reducing T1 relaxation time (Brasch et al. 1984).

The distribution of yellow and red bone marrow strongly influences marrow perfusion. Yellow marrow mainly consists of fat cells and a sparse network of capillaries, venules, and thin-walled veins (Vogler and Murphy 1988). It shows only minor and gradual increase of SI after administration of contrast agents (Erlemann et al. 1988). Red bone marrow includes a rich and arborized vascular network. On contrast-enhanced images, the signal enhancement is rarely obvious on T1-w images without fat suppression since fatty marrow has a high intrinsic SI, which hides the enhancement. It can be detected by careful SI measurements (Vande Berg et al. 1998).

Studies showed, that bone marrow perfusion decreases with age (Baur et al. 1997; Chen et al.

2001; Montazel et al. 2003; Griffith et al. 2005), an increasing fat content corresponds to a decrease of marrow perfusion (Bluemke et al. 1995; Montazel et al. 2003; Griffith et al. 2005), and perfusion is higher in the upper compared to the lower lumbar spine (Savvopoulou et al. 2008).

For the correct interpretation of a perfusion analysis, it is useful to know the distribution pattern between the water and fat component in the assessed vertebral bone marrow. Otherwise, an increase/decrease of the fat component might be falsely interpreted as a decrease/increase of perfusion due to a pathologic cause (Biffar et al. 2010c, d). Initial studies assessing the value of DCE-MRI in the discrimination of benign and malignant vertebral fractures semi-quantitatively examined the perfusion of bone marrow using descriptive parameters like the peak contrast-enhancement percentage, enhancement slope, and time-intensity-curve (TIC) patterns based on operator-defined regions of interest (ROIs) (Chen et al. 2002; Tokuda et al. 2005).

The observed TICs can be classified into five groups:
A: nearly flat TIC,
B: slow inclination curve,
C: rapidly rising slope (wash-in) during early phase, followed by a plateau after the peak enhancement is achieved,
D: rapidly rising slope (wash-in) during the initial short period like in type C, followed by a wash-out phase,
E: initially rapidly rising slope followed by a second slow-rising phase.

If the difference in maximal enhancement and SI at the endpoint is greater than 20% of baseline SI, a type C curve is defined as either type D or type E, depending on the wash-in or wash-out of contrast (Chen et al. 2002; Tokuda et al. 2005).

Chen et al. (2002) examined 42 patients with acute compression fractures ($n = 12$), chronic compression fractures ($n = 21$), and metastatic vertebral lesions with ($n = 6$) or without ($n = 32$) compression fracture. A type D curve was highly predictive (positive predictive value 100%) for a metastatic lesion with or without fracture, since the packed viable tumor cells are thought to lead to an early wash-out because of scarcity of matrix. But since the type D curve was found in only one-third (18 out of 38) of malignant lesions, the sensitivity for diagnosing malignant vertebral lesions was not regarded to be sufficiently high.

A type E curve was predictive for benign acute or chronic compression fractures (positive predictive value 85.7%), because an increase in vascularity, infiltration of inflammatory cells, vasodilatation, and exudation of plasma is thought to result in extravasation of more contrast agent into the extracapillary space without balanced venous wash-out. But since only 6 out of 33 (18.2%) of the vertebral compression fractures showed a type E curve, its sensitivity for diagnosing benign vertebral compression fractures is also low. There were no significant differences for peak enhancement percentage and enhancement slope with overlapping areas between benign and malignant lesions.

Another study performed by Tokuda et al. (2005) found some contradictory results with TIC patterns not being able to distinguish between benign and malignant lesions. They examined patients with osteoporotic compression fractures ($n = 8$) with ages of the fractures ranging from 27 to 45 days, benign vertebral lesions (giant cell tumor, avascular necrosis, tuberculous spondylitis, Schmorl's nodes, vertebral hemangioma) without compression fractures ($n = 11$), and metastatic vertebral lesions with ($n = 8$) and without ($n = 21$) compression fractures. Type E curves were not only seen in benign fractures, but also observed in metastatic vertebral lesions without compression fracture. Type D lesions were also nonspecific. In this study, peak enhancement, steepest slope, and slope were significantly higher in pathologic compression fractures, than in osteoporotic fractures. The authors hypothesize that this difference might be because of the time delay (27–45 days) from fracture to imaging: if osteoporotic fractures are examined in the early phase of healing during the inflammatory phase (like those of Chen et al. 2002), an increase in vascularity might show higher peak enhancement, steepest slope, and slope, comparable with those of pathologic compression fractures. But unfortunately, this study does not provide information about the exact sensitivities and specificities of the examined parameters, and the study subgroup population was small.

Since studies based on semi-quantitative parameters revealed discrepant results and depend on well-known limitations, like a dependence on examination parameters like the injection protocol and an unclear interpretation in terms of hemodynamic parameters (Biffar et al. 2010c, d), another approach quantitatively analyzes the dynamic contrast-enhanced data and directly assesses the perfusion and endothelial permeability using high temporal resolution T1w-MRI.

Therefore, the tissue concentration–time curve is derived from the signal–time curve assuming a linear relationship between the concentration of the tracer and T1 and a known functional dependence between the signal intensity and T1. In a second step, the perfusion- and/or permeability parameters are determined with tracer-kinetic analysis, which provides a relation between the hemodynamic parameters and the measured TICs (Jaquez 1985; Tofts et al. 1999; Brix et al. 2004). The quantitative analysis requires the additional measurement of an arterial input function (AIF) in the feeding artery to correct variations of the tissue concentration, which are not directly related to the hemodynamic state of the tissue itself (injection rate, bolus shape, etc.) (Biffar et al. 2010b). The AIF can be obtained using a circular ROI in the aortic lumen, and can be calculated as the relative signal enhancement divided by (1−hematocrit) to derive the plasma concentrations (Biffar et al. 2010c, d). Most studies used an arbitrary hematocrit value of 0.45, since exact values for individual patients were not always available (Biffar et al. 2010c, d, 2011).

The current standard model in tracer-kinetic analysis of DCE-MRI produces a parameter K^{trans} that represents a mixture of perfusion and permeability (Tofts et al. 1999). Using a two-compartment model (Brix et al. 2004) or a distributed parameter model (Buckley et al. 2004), perfusion and permeability can be fully separated. Four independent perfusion parameters can be derived, characterizing the degree of vascularity and capillary perfusion, plasma flow (PF), plasma volume (PV), extraction flow (EF), and the interstitial volume.

Initial examinations evaluated the potential of the quantitative assessment of DCE-MRI in osteoporotic fractures. Biffar et al. (2010c, d) showed in 20 patients with acute osteoporotic compression fractures that perfusion is strongly increased compared to normal appearing bone marrow. In the same study, quantitative DW-MRI (ADC values) was compared with the perfusion parameters. IV and ADC value positively correlated, confirming the assumption that ADC is essentially determined by the diffusion of water in the extracellular space, and that intracellular water has a weaker contribution. The negative correlation of PV

and ADC may be explained firstly by the fact that the perfusion effects have been eliminated by the choice of the *b-values*, and secondly by the fact that an increase of the PV leads to a decrease of the IV. In normal appearing bone marrow, the interstitial compartment is most likely bigger than the intravascular compartment, because the TIC did not reproduce the AIF. The shape of the TIC suggested that normal appearing bone marrow corresponds to the intermediate regime of contrast agent exchange between both compartments.

Other studies showed, that quantitative DCE-MRI can successfully be used to differentiate between normal and diseased vertebral bone marrow (Biffar et al. 2010c, d, 2011). The use of tracer-kinetic models might be useful in the differentiation of benign and malignant vertebral fractures, studies on this purpose are still ongoing.

3.4 FDG-PET/PET-CT

Fluorodeoxyglucose positron emission tomography (FDG-PET) visualizes the increased glucose metabolism that occurs in malignant and inflammatory lesions, and has been used extensively to differentiate malignant tumors from benign lesions in many organ systems (Strauss and Conti 1991; Hoh et al. 1997). While tumor cells typically accumulate FDG, osteoporotic fractures are not expected to accumulate a high amount of FDG, which may allow differentiation between benign and malignant compression fractures (Bredella et al. 2008). False-positive results can occur in patients who have been treated with bone marrow stimulating agents. One to two months after treatment, FDG-uptake is expected to return to normal (Bredella et al. 2008). Osteomyelitis and discitis can show an increased uptake, mimicking malignancy (Guhlmann et al. 1998a, b; Schmitz et al. 2002). Chronic fractures have also been reported to show a high FDG accumulation due to infiltration with macrophages and granulation tissue (Palmer et al. 1995; Guhlmann et al. 1998a, b).

For this reason, the patient's clinical history should be actively sought when interpreting positive findings, especially in cases with diffuse osseous uptake, mimicking a diffuse osseous process (Bredella et al. 2008). In PET-CT, the CT portion improves the exact fracture localization and provides additional information on fracture morphology (Metser et al. 2004; Bredella et al. 2008).

Kato et al. (2003) examined 10 patients with acute benign vertebral fractures, 9 patients with acute malignant, and one patient with both acute benign and malignant vertebral compression fractures. FDG-PET showed significant differences ($p = 0.0006$) between benign and malignant vertebral compression fractures with a mean SUV of 1.36 ± 0.49 (SD) in the benign, and 4.46 ± 2.12 (SD) in the malignant group. No significant correlation was noted between the histologic type of primary malignant tumor and FDG accumulation of the metastatic lesion. At a cut-off value of SUV 2.0, a sensitivity of 80%, a specificity of 88.9%, and an accuracy of 85.7% could be shown.

Bredella et al. (2008) retrospectively evaluated the use of FDG-PET and FDG-PET-CT in differentiating benign from malignant compression fractures. The neoplastic fractures were due to different underlying malignancies, e.g. leukemia, ovarian cancer, or esophageal cancer. There were 21 patients with 29 benign, and 12 patients with 14 malignant compression fractures. Only 5 of the benign fractures were acute, based on clinical history and imaging characteristics on additionally evaluated MRI scans. The age of the other fractures was not listed in the study.

Malignant fractures demonstrated intense radiotracer uptake and a mean standardized uptake value (SUV) of 3.99 ± 1.52, while benign compression fractures showed only mildly increased or no increased uptake of FDG-PET and a mean SUV of 1.94 ± 0.97, leading to significant differences for the standardized uptake values (SUV) for benign and malignant fractures. Acute and chronic benign fractures could not be differentiated. FDG-PET showed a sensitivity of 86%, a specificity of 83%, a positive predictive value of 84%, a negative predictive value of 71% and an accuracy of 92% (Bredella et al. 2008). In this study some of the false-positive results were found in patients that had been treated with marrow-stimulating agents resulting in an increased FDG-PET uptake (Bredella et al. 2008), what was consistent with the effects described in previous studies (Aoki et al. 2003). Therefore in interpreting positive findings, possible treatment with marrow-stimulating agents should be verified. In contrast to bone scintigraphy, where there is an increased uptake
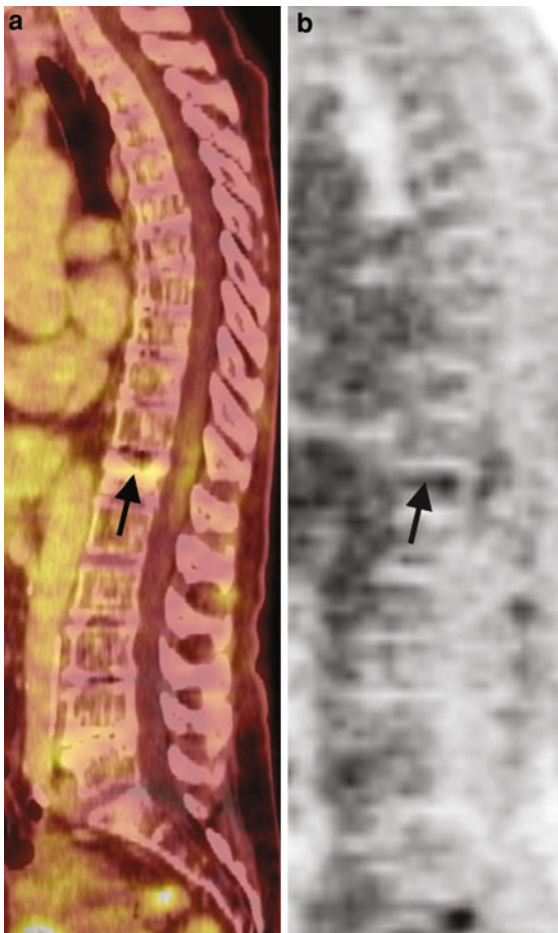
Fig. 16 62-year-old patient with a fracture of Th 12 due to osteoporosis. Sagittal FDG-PET-CT fusion image (**a**) showing a fracture of the upper vertebral cover plate of Th 12 with an adjacent band-like increased uptake (SUV 1.2), that is also depicted in the PET image (**b**)

Fig. 17 67-year-old patient with a malignant fracture due to metastasis of a neuroendocrinal tumor. Sagittal Ga^{68}-DOTA-TATE PET-CT fusion image (**a**) showing a heavily increased tracer uptake in a wedge-shaped vertebral fracture (*arrow*). There is also an increased uptake in the other non-fractured vertebral bodies due to metastases, as can also be seen in the PET image (**b**)

for many months (Masala et al. 2005), in FDG-PET there is only a mild to moderately increased uptake in acute benign fractures, while chronic benign fractures show no or only mildly increased uptake (Bredella et al. 2008).

Figures 16 and 17 show PET-CT images of an osteoporotic and a malignant vertebral fracture.

FDG-PET is recommended not as a screening test, but rather as an additional imaging modality in problem cases, with the possibility to evaluate the entire skeletal system in search for metastatic disease. Patients with contraindications to MRI (pacemakers, claustrophobia, severe pain) can profit from FDG-PET(-CT) (Bredella et al. 2008).
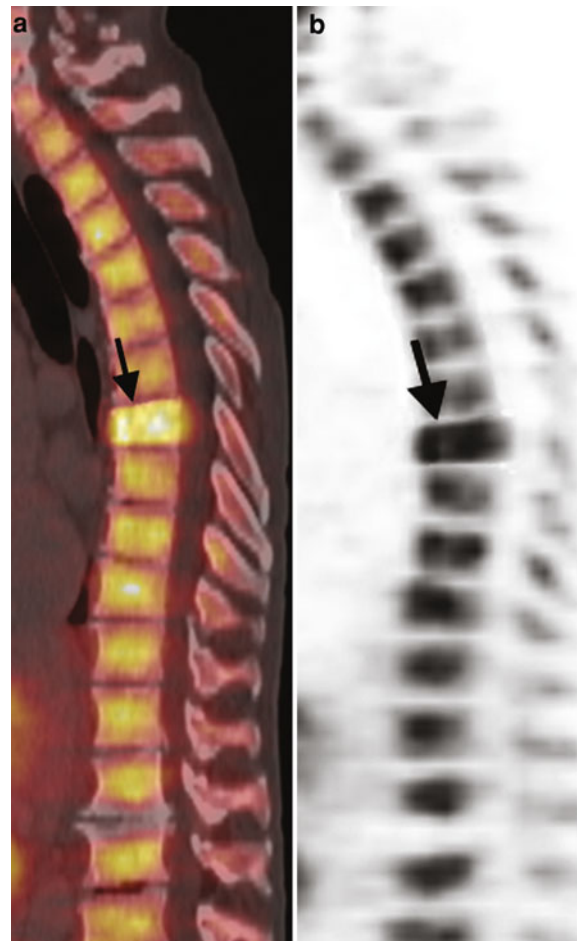
3.5 Scintigraphy/SPECT

Scintigraphy and single-photon emission computed tomography (SPECT) use the emission of radiation of radiopharmaceuticals, which aggregate in areas of high metabolism.

Bone Technetium-99 hydroxymethylene diphosphonate (Tc-99 HMDP) scintigraphy is an established screening method for skeletal metastases. Multiple increased uptakes are often considered as suspicious for malignancy, while a solitary increased uptake of the fractured vertebra is observed in most recent benign and malignant fractures (Taoka et al. 2001).

Acute vertebral compression fractures, degenerative, and inflammatory diseases show similar radionuclide dynamics of Tc-99 HMDP, which leads to a lack of sensitivity in differentiating benign from malignant vertebral compression fractures.

Tokuda et al. (2011) examined 53 malignant vertebral compression fractures in 51 patients, and 44 acute benign vertebral compression fractures in 40 patients to compare the diagnostic value of SPECT with Tc-99 HMDP and morphologic MRI features. The results showed, that the overall accuracy of MRI was significantly greater than that of the SPECT images for both observers in the study. In vertebral compression fractures with partial replacement of the fatty marrow, MRI performed significantly better in differentiating between the two entities. However, fractures with a complete replacement of fatty marrow did not show significant differences between the sensitivities (up to 87.1% for SPECT, up to 94.9% for MRI), specificities (up to 89.5% for SPECT, up to 89.5% for MRI) and accuracies (up to 91.4% for SPECT, up to 91.4% for MRI) of both techniques. Therefore the authors suggested, that SPECT represents a valid alternative to MR imaging for differentiating malignant from benign vertebral compression fractures in patients, which are not able to undergo MRI due to contraindications, like cardiac pacemakers. MRI should still be used for patients without contraindications.

Thariat et al. (2004) used Thallium-201 chloride (^{201}TI), which is a radionuclide with gamma-ray emission that is mainly used as a myocardial perfusion marker, for the differentiation of benign and malignant vertebral fractures that were not older than 3 months. Conventional bone scintigraphy and SPECT were performed. The authors showed a weak sensitivity (28.6%), which did not support its systematic use to distinguish benign from malignant recent vertebral fractures. SPECT showed unchanged results in comparison with conventional bone scintigraphy. But its high specificity (92.9% on early, and 100% on delayed images) may make ^{201}TI-scintigraphy or -SPECT a valuable tool to avoid any unnecessary invasive procedure, if performed prior to vertebral biopsy. In contrast to other studies that found a higher sensitivity in the evaluation of other soft tissues and peripheral bone tumors, the authors hypothesize that the soft tissues around the vertebrae might have attenuated the radionuclide gamma-rays in a much higher extent than expected, or that edema, necrosis, and an altered vascularization in vertebral fractures hamper the spread of ^{201}TI, which has been shown an accurate indicator of the viability, metabolic activity, and vascularization of tumors.

4 Therapy

Relieving pain and preserving mobility are the most important goals that may require short-term analgesic therapy in vertebral compression fractures. In cases of severe pain due to osteoporotic vertebral fracture hospitalization can be justified (Burge et al. 2002). Although there is a lack of randomized trials, analgesics, nonsteroidal anti-inflammatory drugs, and drugs relieving neuropathic pain are commonly used for the therapy of patients with acute osteoporotic vertebral fractures. Narcotics facilitate mobility and avoid a prolonged bed rest (Prather et al. 2007). Spinal orthoses can reduce pain and disability in the first weeks after a vertebral fracture (Pfeifer et al. 2004; Stadhouder et al. 2009). Therapeutic exercise programs may reduce pain and improve functional status, but the findings are not constant across studies (Dusdal et al. 2011). An adequate intake of vitamin D is recommended in patients with osteoporosis (Lips et al. 2010). Several pharmacotherapies, like bisphosphonates (MacLean et al. 2008), selective estrogen receptor modulators (MacLean et al. 2008; Silverman et al. 2008; Cummings et al. 2010), denosumab (Cummings et al. 2009), or strontium ranelate (Meunier et al. 2004) have shown efficacy in reducing the risk of vertebral fractures.

Therapeutic options for patients with pathological vertebral body fractures include medical therapy and surgical intervention. Non-steroidal anti-inflammatory drugs and steroids can be applied against bone pain, neuropathic drugs can be used for nerve root pain. Nonresponsive patients can be treated with radiotherapy, but mechanical instability is not corrected in these cases. Open surgical procedures are highly invasive and may offer an unfavorable risk/benefit ratio. Vertebroplasty and kyphoplasty are an favorable option in patients with malignant vertebral compression fractures that do not cause neurological deficits but compromise quality of live because of intractable pain (Tancioni et al. 2011).

Vertebroplasty and kyphoplasty are partly indicated for treatment of painful primary and secondary osteoporotic vertebral compression fractures refractory to conservative therapy (Kondo 2008), although in the last two years some studies questioned its usefulness (Buchbinder et al. 2009; Kallmes et al. 2009; Buchbinder and Kallmes 2010).

In percutaneous vertebroplasty (PVP) a cement substance with polymethylmethacrylate (PMMA) is injected into a collapsed vertebral body under fluoroscopic control resulting in structural stabilization (Kondo 2008). In kyphoplasty, prior to the injection of PMMA, an inflatable bone tamp is used to erect the collapsed vertebral body and minimize the kyphotic deformity (Lieberman et al. 2001). In osteoporotic fractures, the procedure is mostly done after 2–6 weeks of conservative treatment, but some practitioners favor an earlier intervention, because they believe that besides pain relief, the kyphotic deformity should be corrected, as it might increase the risk of future fractures due to an altered spinal load distribution (Gaitanis et al. 2005). Mechanical stabilization, which prevents further micro motion of the vertebral fracture and provides realignment of the anterior and posterior ligaments, as well as damage of local pain receptors due to the unreacted cytotoxic methacrylate monomer and the heat from the polymerization of PMMA, are discussed as possible mechanisms of pain relieve (Belkoff and Molloy 2003). More than 90% of patients show an immediate pain relief, and about 50% of the patients report decreased pain during the immediate postoperative period. Significant differences in the clinical outcome between vertebroplasty and kyphoplasty could not yet been shown, despite theoretical benefits of the correction of height and deformity (Gill et al. 2007). Both techniques exhibit relatively low complication rates from 1 to 3% in osteoporotic and up to 10% in tumor-related vertebral compression fractures. Possible complications are related to needle displacement, cement extravasation, infection, bleeding, or iatrogenic fractures (Kondo 2008).

If there are multiple compression fractures or chronic fractures, the correct vertebra can be identified by depicting the bone marrow in MRI. Tanigawa et al. (2006) showed, that patients with extensive bone marrow edema in the vertebral bodies that underwent vertebroplasty, showed a significantly greater clinical improvement than those without this pattern. This shows agreement with other studies that showed effectiveness in chronic fractures, but even better clinical outcomes in patients with acute compression fractures (Brown et al. 2004), because older vertebral compression fractures lose bone marrow edema pattern.

Voormolen et al. (2006) also found a more frequent decrease of pain in patients with observed BME, but also found that 71% of the patients without BME showed clinical improvement, so that the authors postulated that vertebroplasty should not be withheld based on absence of BME alone.

Two randomized, double-blind trials (Buchbinder et al. 2009; Kallmes et al. 2009) compared vertebroplasty with a sham procedure in patients with painful vertebral fractures, that had been identified within 12 months, and found no beneficial effects from vertebroplasty with respect to pain, quality of life, and functional disability. The mean duration of symptoms before the procedure was 12–13 weeks in one study (Buchbinder et al. 2009), and 16–20 weeks in the other (Kallmes et al. 2009). Analyses did not indicate that vertebroplasty was more beneficial than the sham procedure within the subgroup of patients with pain of shorter duration, although vertebroplasty and kyphoplasty have been proposed to be most effective for acute fracture pain.

Since new vertebral compression fractures often occur relatively soon after intervention in vertebral bodies adjacent to fractured vertebral bodies treated with vertebroplasty (Uppin et al. 2003), there is special interest in the possibility to predict new adjacent-level compression fractures to justify a prophylactic vertebroplasty there. Sugimoto et al. (2008) showed, that collapsed vertebral bodies adjacent to vertebral bodies treated with PVP show significantly higher ADCs than not collapsed vertebral bodies prior to PVP, indicating that DWI before PVP might be a predictor for new compression fractures following PVP.

Therefore, the treatment of acute vertebral collapse should be planned in an interdisciplinary team setting, taking into account conservative management as well as surgical treatment. Due to the contradictory results, vertebroplasty should only be performed in those cases where pain cannot be managed conservatively and bone marrow edema is still present.

References

An HS, Andreshak TG et al (1995) Can we distinguish between benign versus malignant compression fractures of the spine by magnetic resonance imaging? Spine (Phila Pa 1976) 20(16): 1776–1782

Aoki J, Endo K et al (2003) FDG-PET for evaluating musculo-skeletal tumors: a review. J Orthop Sci 8(3):435–441

Baker LL, Goodman SB et al (1990) Benign versus pathologic compression fractures of vertebral bodies: assessment with conventional spin-echo, chemical-shift, and STIR MR imaging. Radiology 174(2):495–502

Batson OV (1940) The function of the vertebral veins and their role in the spread of metastases. Ann Surg 112(1):138–149

Baur A, Stabler A et al (1997) MRI gadolinium enhancement of bone marrow: age-related changes in normals and in diffuse neoplastic infiltration. Skelet Radiol 26(7):414–418

Baur A, Stabler A et al (1998) Diffusion-weighted MR imaging of bone marrow: differentiation of benign versus pathologic compression fractures. Radiology 207(2):349–356

Baur A, Huber A et al (2001) Diagnostic value of increased diffusion weighting of a steady-state free precession sequence for differentiating acute benign osteoporotic fractures from pathologic vertebral compression fractures. Am J Neuroradiol 22(2):366–372

Baur A, Huber A et al (2002a) Differentiation of benign osteoporotic and neoplastic vertebral compression fractures with a diffusion-weighted, steady-state free precession sequence. RoFo : Fortschritte auf dem Gebiete der Rontgenstrahlen und der Nuklearmedizin 174(1):70–75

Baur A, Stabler A et al (2002b) Acute osteoporotic and neoplastic vertebral compression fractures: fluid sign at MR imaging. Radiology 225(3):730–735

Baur A, Dietrich O et al (2003) Diffusion-weighted imaging of bone marrow: current status. Eur Radiol 13(7):1699–1708

Belkoff SM, Molloy S (2003) Temperature measurement during polymerization of polymethylmethacrylate cement used for vertebroplasty. Spine 28(14):1555–1559

Bhalla S, Reinus WR (1998) The linear intravertebral vacuum: a sign of benign vertebral collapse. Am J Roentgenol 170(6): 1563–1569

Biffar A, Baur-Melnyk A et al (2010a) Multiparameter MRI assessment of normal-appearing and diseased vertebral bone marrow. Eur Radiol 20:2679–2689

Biffar A, Dietrich O et al (2010b) Diffusion and perfusion imaging of bone marrow. Eur J Radiol 76:323–328

Biffar A, Sourbron S et al (2010c) Combined diffusion-weighted and dynamic contrast-enhanced imaging of patients with acute osteoporotic vertebral fractures. Eur J Radiol 76:298–303

Biffar A, Sourbron S et al (2010d) Measurement of perfusion and permeability from dynamic contrast-enhanced MRI in normal and pathological vertebral bone marrow. Magn Reson Med 64(1):115–124

Biffar A, Schmidt GP et al (2011) Quantitative analysis of vertebral bone marrow perfusion using dynamic contrast-enhanced MRI: initial results in osteoporotic patients with acute vertebral fracture. J Magn Reson Imaging 33(3):676–683

Bluemke DA, Petri M et al (1995) Femoral head perfusion and composition: MR imaging and spectroscopic evaluation of patients with systemic lupus erythematosus and at risk for avascular necrosis. Radiology 197(2):433–438

Brasch RC, Weinmann HJ et al (1984) Contrast-enhanced NMR imaging: animal studies using gadolinium-DTPA complex. Am J Roentgenol 142(3):625–630

Bredella MA, Essary B et al (2008) Use of FDG-PET in differentiating benign from malignant compression fractures. Skelet Radiol 37(5):405–413

Brix G, Kiessling F et al (2004) Microcirculation and microvasculature in breast tumors: pharmacokinetic analysis of dynamic MR image series. Magn Reson Med 52(2): 420–429

Brown DB, Gilula LA et al (2004) Treatment of chronic symptomatic vertebral compression fractures with percutaneous vertebroplasty. Am J Roentgenol 182(2):319–322

Buchbinder R, Kallmes DF (2010) Vertebroplasty: when randomized placebo-controlled trial results clash with common belief. Spine J (Official journal of the North American Spine Society) 10(3):241–243

Buchbinder R, Osborne RH et al (2009) A randomized trial of vertebroplasty for painful osteoporotic vertebral fractures. N Engl J Med 361(6):557–568

Buckley DL, Roberts C et al (2004) Prostate cancer: evaluation of vascular characteristics with dynamic contrast-enhanced T1-weighted MR imaging—initial experience. Radiology 233(3):709–715

Burge R, Puleo E et al (2002) Inpatient hospital and post-acute care for vertebral fractures in women. Value Health (Journal of the International Society for Pharmacoeconomics and Outcomes Research) 5(4):301–311

Castillo M, Arbelaez A et al (2000) Diffusion-weighted MR imaging offers no advantage over routine noncontrast MR imaging in the detection of vertebral metastases. Am J Neuroradiol 21(5):948–953

Chan JH, Peh WC et al (2002) Acute vertebral body compression fractures: discrimination between benign and malignant causes using apparent diffusion coefficients. Br J Radiol 75(891):207–214

Chen WT, Shih TT et al (2001) Vertebral bone marrow perfusion evaluated with dynamic contrast-enhanced MR imaging: significance of aging and sex. Radiology 220(1): 213–218

Chen WT, Shih TT et al (2002) Blood perfusion of vertebral lesions evaluated with gadolinium-enhanced dynamic MRI: in comparison with compression fracture and metastasis. J Magn Reson Imaging 15(3):308–314

Constans JP, de Divitiis E et al (1983) Spinal metastases with neurological manifestations: review of 600 cases. J Neurosurg 59(1):111–118

Cuenod CA, Laredo JD et al (1996) Acute vertebral collapse due to osteoporosis or malignancy: appearance on unenhanced and gadolinium-enhanced MR images. Radiology 199(2):541–549

Cummings SR, San Martin J et al (2009) Denosumab for prevention of fractures in postmenopausal women with osteoporosis. N Engl J Med 361(8):756–765

Cummings SR, Ensrud K et al (2010) Lasofoxifene in postmenopausal women with osteoporosis. N Engl J Med 362(8):686–696

Dietrich O, Biffar A et al (2009) Diffusion-weighted imaging of bone marrow. Semin Musculoskelet Radiol 13(2):134–144

Dusdal K, Grundmanis J et al (2011) Effects of therapeutic exercise for persons with osteoporotic vertebral fractures: a systematic review. Osteoporos Int (Journal established as result of cooperation between the European Foundation for Osteoporosis and the National Osteoporosis Foundation of the USA) 22(3):755–769

Eastell R (2007) Breast cancer and the risk of osteoporotic fracture: a paradox. J Clin Endocrinol Metab 92(1):42–43

Eito K, Waka S et al (2004) Vertebral neoplastic compression fractures: assessment by dual-phase chemical shift imaging. J Magn Reson Imaging 20(6):1020–1024

Erlemann R, Reiser M et al (1988) Time-dependent changes in signal intensity in neoplastic and inflammatory lesions of the musculoskeletal system following intravenous administration of Gd-DTPA. Der Radiologe 28(6):269–276

Erly WK, Oh ES et al (2006) The utility of in-phase/opposed-phase imaging in differentiating malignancy from acute benign compression fractures of the spine. Am J Neuroradiol 27(6):1183–1188

Fornasier VL, Czitrom AA (1978) Collapsed vertebrae: a review of 659 autopsies. Clin Orthop Relat Res 131:261–265

Frager D, Elkin C et al (1988) Subacute osteoporotic compression fracture: misleading magnetic resonance appearance. Skelet Radiol 17(2):123–126

Gagnerie F, Taillan B et al (1987) Intravertebral vacuum phenomenon in multiple myeloma. Clin Rheumatol 6(4):597–599

Gaitanis IN, Carandang G et al (2005) Restoring geometric and loading alignment of the thoracic spine with a vertebral compression fracture: effects of balloon (bone tamp) inflation and spinal extension. Spine J 5(1):45–54

Genant HK, Wu CY et al (1993) Vertebral fracture assessment using a semiquantitative technique. J Bone Miner Res 8(9):1137–1148

Gill JB, Kuper M et al (2007) Comparing pain reduction following kyphoplasty and vertebroplasty for osteoporotic vertebral compression fractures. Pain Physician 10(4):583–590

Golimbu C, Firooznia H et al (1986) The intravertebral vacuum sign. Spine (Phila Pa 1976) 11(10):1040–1043

Griffith JF, Yeung DK et al (2005) Vertebral bone mineral density, marrow perfusion, and fat content in healthy men and men with osteoporosis: dynamic contrast-enhanced MR imaging and MR spectroscopy. Radiology 236(3):945–951

Guhlmann A, Brecht-Krauss D et al (1998a) Chronic osteomyelitis: detection with FDG PET and correlation with histopathologic findings. Radiology 206(3):749–754

Guhlmann A, Brecht-Krauss D et al (1998b) Fluorine-18-FDG PET and technetium-99 m antigranulocyte antibody scintigraphy in chronic osteomyelitis. J Nucl Med 39(12):2145–2152

Hacklander T, Scharwachter C et al (2006) Value of diffusion-weighted imaging for diagnosing vertebral metastases due to prostate cancer in comparison to other primary tumors. RoFo: Fortschritte auf dem Gebiete der Rontgenstrahlen und der Nuklearmedizin 178(4):416–424

Harrington KD (1986) Metastatic disease of the spine. J Bone Joint Surg Am 68(7):1110–1115

Hasegawa K, Homma T et al (1998) Vertebral pseudarthrosis in the osteoporotic spine. Spine (Phila Pa 1976) 23(20):2201–2206

Herneth AM, Friedrich K et al (2005) Diffusion weighted imaging of bone marrow pathologies. Eur J Radiol 55(1):74–83

Hoh CK, Schiepers C et al (1997) PET in oncology: will it replace the other modalities? Semin Nucl Med 27(2):94–106

Ishiyama M, Fuwa S et al (2010) Pedicle involvement on MR Imaging is common in osteoporotic compression fractures. Am J Neuroradiol 31(4):668–673

Jaquez JA (1985) Compartmental analysis in biology and medicine. The university of Michigan Press, Ann Arbor

Jung HS, Jee WH et al (2003) Discrimination of metastatic from acute osteoporotic compression spinal fractures with MR imaging. Radiographics 23(1):179–187

Kallmes DF, Comstock BA et al (2009) A randomized trial of vertebroplasty for osteoporotic spinal fractures. N Engl J Med 361(6):569–579

Kaplan PA, Orton DF et al (1987) Osteoporosis with vertebral compression fractures, retropulsed fragments, and neurologic compromise. Radiology 165(2):533–535

Karchevsky M, Babb JS et al (2008) Can diffusion-weighted imaging be used to differentiate benign from pathologic fractures? a meta-analysis. Skelet Radiol 37(9):791–795

Kato K, Aoki J et al (2003) Utility of FDG-PET in differential diagnosis of benign and malignant fractures in acute to subacute phase. Ann Nucl Med 17(1):41–46

Kondo KL (2008) Osteoporotic vertebral compression fractures and vertebral augmentation. Sem Intervent Radiol 25(4):413–424

Kubota T, Yamada K et al (2005) High-resolution imaging of the spine using multidetector-row computed tomography: differentiation between benign and malignant vertebral compression fractures. J Comput Assist Tomogr 29(5):712–719

Kumpan W, Salomonowitz E et al (1986) The intravertebral vacuum phenomenon. Skelet Radiol 15(6):444–447

Lafforgue P, Chagnaud C et al (1997) The intravertebral vacuum phenomenon ("vertebral osteonecrosis"): migration of intradiscal gas in a fractured vertebral body. Spine (Phila Pa 1976) 22(16):1885–1891

Laredo JD, Lakhdari K et al (1995) Acute vertebral collapse: CT findings in benign and malignant nontraumatic cases. Radiology 194(1):41–48

Le Bihan DJ (1998) Differentiation of benign versus pathologic compression fractures with diffusion-weighted MR imaging: a closer step toward the "holy grail" of tissue characterization? Radiology 207(2):305–307

Lecouvet FE, Vande Berg BC et al (1997) Vertebral compression fractures in multiple myeloma: part I: distribution and appearance at MR imaging. Radiology 204(1):195–199

Leeds NE, Kumar AJ et al (2000) Magnetic resonance imaging of benign spinal lesions simulating metastasis: role of diffusion-weighted imaging. Top Magn Reson Imaging 11(4):224–234

Lieberman IH, Dudeney S et al (2001) Initial outcome and efficacy of "kyphoplasty" in the treatment of painful osteoporotic vertebral compression fractures. Spine 26(14):1631–1638

Link TM, Guglielmi G et al (2005) Radiologic assessment of osteoporotic vertebral fractures: diagnostic and prognostic implications. Eur Radiol 15(8):1521–1532

Linn J, Birkenmaier C et al (2009) The intravertebral cleft in acute osteoporotic fractures: fluid in magnetic resonance imaging-vacuum in computed tomography? Spine 34(2):E88–E93

Lips P, Bouillon R et al (2010) Reducing fracture risk with calcium and vitamin D. Clin Endocrinol 73(3):277–285

MacLean C, Newberry S et al (2008) Systematic review: comparative effectiveness of treatments to prevent fractures in men and women with low bone density or osteoporosis. Ann Intern Med 148(3):197–213

Malghem J, Maldague B et al (1993) Intravertebral vacuum cleft: changes in content after supine positioning. Radiology 187(2):483–487

Masala S, Schillaci O et al (2005) MRI and bone scan imaging in the preoperative evaluation of painful vertebral fractures treated with vertebroplasty and kyphoplasty. In Vivo 19(6):1055–1060

Melton LJ (1997) Epidemiology of spinal osteoporosis. Spine (Phila Pa 1976) 22(24 Suppl):2S–11S

Metser U, Lerman H et al (2004) Malignant involvement of the spine: assessment by 18F-FDG PET/CT. J Nucl Med 45(2):279–284

Meunier PJ, Roux C et al (2004) The effects of strontium ranelate on the risk of vertebral fracture in women with postmeno-pausal osteoporosis. N Engl J Med 350(5):459–468

Montazel JL, Divine M et al (2003) Normal spinal bone marrow in adults: dynamic gadolinium-enhanced MR imaging. Radiology 229(3):703–709

Moulopoulos LA, Yoshimitsu K et al (1996) MR prediction of benign and malignant vertebral compression fractures. J Magn Reson Imaging 6(4):667–674

Moulopoulos LA, Dimopoulos MA et al (1999) Bone lesions with soft-tissue mass: magnetic resonance imaging diagno-sis of lymphomatous involvement of the bone marrow versus multiple myeloma and bone metastases. Leuk Lymph 34(1–2):179–184

O'Neill TW, Felsenberg D et al (1996) The prevalence of vertebral deformity in European men and women: the European vertebral osteoporosis study. J Bone Miner Res (Official journal of the American Society for Bone and Mineral Research) 11(7):1010–1018

Oztekin O, Ozan E et al (2009) SSH-EPI diffusion-weighted MR imaging of the spine with low b values: is it useful in differentiating malignant metastatic tumor infiltration from benign fracture edema? Skelet Radiol 38(7):651–658

Palmer WE, Rosenthal DI et al (1995) Quantification of inflammation in the wrist with gadolinium-enhanced MR imaging and PET with 2-[F-18]-fluoro-2-deoxy-D-glucose. Radiology 196(3):647–655

Park SW, Lee JH et al (2004) Single shot fast spin echo diffusion-weighted MR imaging of the spine; is it useful in differentiating malignant metastatic tumor infiltration from benign fracture edema? Clin Imaging 28(2):102–108

Pfeifer M, Begerow B et al (2004) Effects of a new spinal orthosis on posture, trunk strength, and quality of life in women with postmenopausal osteoporosis: a randomized trial. Am J Phys Med Rehabil / Assoc Acad Physiatrists 83(3):177–186

Prather H, Watson JO et al (2007) Nonoperative management of osteoporotic vertebral compression fractures. Injury 38(Suppl 3):S40–S48

Ragab Y, Emad Y et al (2009) Differentiation of osteoporotic and neoplastic vertebral fractures by chemical shift in-phase and out-of phase MR imaging. Eur J Radiol 72(1):125–133

Resnick D, Niwayama G et al (1981) Spinal vacuum phenomena: anatomical study and review. Radiology 139(2):341–348

Rupp RE, Ebraheim NA et al (1995) Magnetic resonance imaging differentiation of compression spine fractures or vertebral lesions caused by osteoporosis or tumor. Spine (Phila Pa 1976) 20(23):2499–2503 discussion 2504

Sartoris DJ, Clopton P et al (1986) Vertebral-body collapse in focal and diffuse disease: patterns of pathologic processes. Radiology 160(2):479–483

Sattari A, Quillard A et al (2008) Benign nontraumatic osteolytic vertebral collapse simulating malignancy. Eur Radiol 18(3):631–638

Savvopoulou V, Maris TG et al (2008) Differences in perfusion parameters between upper and lower lumbar vertebral segments with dynamic contrast-enhanced MRI (DCE MRI). Eur Radiol 18(9):1876–1883

Schmitz A, Risse JH et al (2002) FDG-PET findings of vertebral compression fractures in osteoporosis: preliminary results. Osteoporos Int 13(9):755–761

Shih TT, Huang KM et al (1999) Solitary vertebral collapse: distinction between benign and malignant causes using MR patterns. J Magn Reson Imaging 9(5):635–642

Silverman SL, Christiansen C et al (2008) Efficacy of bazedoxifene in reducing new vertebral fracture risk in postmenopausal women with osteoporosis: results from a 3-year, randomized, placebo-, and active-controlled clinical trial. J Bone Miner Res (Official journal of the American Society for Bone and Mineral Research) 23(12):1923–1934

Stäbler A, Schneider P et al (1999) Intravertebral vacuum phenomenon following fractures: CT study on frequency and etiology. J Comput Assist Tomogr 23(6):976–980

Stadhouder A, Buskens E et al (2009) Nonoperative treatment of thoracic and lumbar spine fractures: a prospective randomized study of different treatment options. J Orthop Trauma 23(8):588–594

Strauss LG, Conti PS (1991) The applications of PET in clinical oncology. J Nucl Med 32(4):623–648 discussion 649–650

Sugimoto T, Tanigawa N et al (2008) Diffusion-weighted imaging for predicting new compression fractures following percutaneous vertebroplasty. Acta Radiol 49(4):419–426

Tan SB, Kozak JA et al (1991) The limitations of magnetic resonance imaging in the diagnosis of pathologic vertebral fractures. Spine (Phila Pa 1976) 16(8):919–923

Tancioni F, Lorenzetti MA et al (2011) Percutaneous vertebral augmentation in metastatic disease: state of the art. J Support Oncol 9(1):4–10

Tang G, Liu Y et al (2007) Optimization of b value in diffusion-weighted MRI for the differential diagnosis of benign and malignant vertebral fractures. Skelet Radiol 36(11):1035–1041

Tanigawa N, Komemushi A et al (2006) Percutaneous verteb-roplasty: relationship between vertebral body bone marrow edema pattern on MR images and initial clinical response. Radiology 239(1):195–200

Taoka T, Mayr NA et al (2001) Factors influencing visualiza-tion of vertebral metastases on MR imaging versus bone scintigraphy. Am J Roentgenol 176(6):1525–1530

Thariat J, Toubeau M et al (2004) Sensitivity and specificity of thallium-201 scintigraphy for the diagnosis of malignant vertebral fractures. Eur J Radiol 51(3):274–278

Thurnher MM, Bammer R (2006) Diffusion-weighted magnetic resonance imaging of the spine and spinal cord. Semin Roentgenol 41(4):294–311

Tofts PS, Brix G et al (1999) Estimating kinetic parameters from dynamic contrast-enhanced T(1)-weighted MRI of a diffusable tracer: standardized quantities and symbols. J Mag Res Imaging 10(3):223–232

Tokuda O, Hayashi N et al (2005) Dynamic contrast-enhanced perfusion MR imaging of diseased vertebrae: analysis of three parameters and the distribution of the time-intensity curve patterns. Skelet Radiol 34(10):632–638

Tokuda O, Harada Y et al (2011) Malignant versus benign vertebral compression fractures: can we use bone SPECT as a substitute for MR imaging? Nucl Med Commun 32(3):192–198

Uetani M, Hashmi R et al (2004) Malignant and benign compression fractures: differentiation and diagnostic pitfalls on MRI. Clin Radiol 59(2):124–131

Uppin AA, Hirsch JA et al (2003) Occurrence of new vertebral body fracture after percutaneous vertebroplasty in patients with osteoporosis. Radiology 226(1):119–124

Vaccaro AR, Shah SH et al (1999) MRI description of vertebral osteomyelitis, neoplasm, and compression fracture. Orthopedics 22(1):67–73 quiz 74-65

van der Klift M, de Laet CE et al (2004) Risk factors for incident vertebral fractures in men and women: the Rotterdam study. J Bone Miner Res (Official journal of the American Society for Bone and Mineral Research) 19(7):1172–1180

Vande Berg BC, Malghem J et al (1998) Magnetic resonance imaging of the normal bone marrow. Skelet Radiol 27(9):471–483

Vogler JB III, Murphy WA (1988) Bone marrow imaging. Radiology 168(3):679–693

Voormolen MH, van Rooij WJ et al (2006) Pain response in the first trimester after percutaneous vertebroplasty in patients with osteoporotic vertebral compression fractures with or without bone marrow edema. Am J Neuroradiol 27(7):1579–1585

Wasnich RD (1996) Vertebral fracture epidemiology. Bone 18(3 Suppl):179S–183S

White AP, Kwon BK et al (2006) Metastatic disease of the spine. J Am Acad Orthop Surg 14(11):587–598

Yuh WT, Zachar CK et al (1989) Vertebral compression fractures: distinction between benign and malignant causes with MR imaging. Radiology 172(1):215–218

Zajick DC Jr, Morrison WB et al (2005) Benign and malignant processes: normal values and differentiation with chemical shift MR imaging in vertebral marrow. Radiology 237(2):590–596

Zhou XJ, Leeds NE et al (2002) Characterization of benign and metastatic vertebral compression fractures with quantitative diffusion MR imaging. Am J Neuroradiol 23(1):165–170